Detoxification of toxin A and toxin B by copper ion-catalyzed oxidation in production of a toxoid-based vaccine against Clostridioides difficile

Aminzadeh, Aria; Tiwari, Manish Kumar; Mustapha, Srwa Satar Mamah; Navarrete, Sandra Junquera; Henriksen, Anna Bielecka; Møller, Ian Max; Krogfelt, Karen Angeliki; Bjerrum, Morten Jannik; Jørgensen, René

Published in:
Free Radical Biology & Medicine

DOI:
10.1016/j.freeradbiomed.2020.08.021

Publication date:
2020

Document Version
Peer reviewed version

Citation for published version (APA):
Aminzadeh, A., Tiwari, M. K., Mustapha, S. S. M., Navarrete, S. J., Henriksen, A. B., Møller, I. M., Krogfelt, K. A., Bjerrum, M. J., & Jørgensen, R. (2020). Detoxification of toxin A and toxin B by copper ion-catalyzed oxidation in production of a toxoid-based vaccine against *Clostridioides difficile*. *Free Radical Biology & Medicine*, *160*(160), 433-446. https://doi.org/10.1016/j.freeradbiomed.2020.08.021

Detoxification of Toxin A and Toxin B by copper ion-catalyzed oxidation in production of a toxoid-based vaccine against *Clostridioides difficile*

Aria Aminzadeh[1,2,§], Manish Kumar Tiwari[2,§], Srwa Satar Mamah Mustapha[1], Sandra Junquera Navarrete[1], Anna Bielecka Henriksen[1], Ian Max Møller[3], Karen Angeliki Krogfelt[4], Morten Jannik Bjerrum[2,*], René Jørgensen[1,*]

[1]Statens Serum Institut, Department of Bacteria, Parasites and Fungi, Copenhagen, Denmark

[2]University of Copenhagen, Department of Chemistry, Copenhagen, Denmark

[3]Department of Molecular Biology and Genetics, Aarhus University, Forsøgsvej 1, DK-4200 Slagelse, Denmark

[4]Roskilde University, Molecular and Medical Biology, Roskilde Denmark

*Correspondence to: mobj@chem.ku.dk/renj@ssi.dk

René Jørgensen

Statens Serum Institut, Department of Bacteria, Parasites and Fungi,

Artillerivej 5, 2300 Copenhagen S, Denmark

§-These authors equally contributed to this work.

Abstract

Clostridioides difficile infections (CDI) has emerged worldwide as a serious antimicrobial-resistant healthcare-associated disease resulting in diarrhea and pseudomembranous colitis. The two cytotoxic proteins, toxin A (TcdA) and toxin B (TcdB) are the major virulence factor responsible for the disease symptoms. We examined time-dependent oxidative detoxification of TcdA and TcdB using different molar ratios of protein / Cu^{2+} / H_2O_2. The MCO reaction in molar ratios of 1:60:1000 for protein / Cu^{2+} / H_2O_2 at pH 4.5 resulted in a significant 6 $\log_{10}$ fold reduction in cytotoxicity after 120-min incubation at 37 ºC. Circular dichroism revealed that MCO- detoxified TcdA and TcdB had secondary and tertiary structural folds similar to the native proteins. The conservation of immunogenic epitopes of both proteins was tested using monoclonal antibodies in an ELISA, comparing our MCO-detoxification approach to a conventional formaldehyde-detoxification method. The oxidative detoxification of TcdA and TcdB led to an average 2-fold reduction in antibody binding relative to native proteins, whereas formaldehyde cross-linking resulted in 3-fold and 5-fold reductions, respectively. Finally, we show that mice immunized with a vaccine consisting of MCO-detoxified TcdA and TcdB were fully protected against disease symptoms and death following a *C. difficile* infection and elicited substantial serum IgG responses against both TcdA and TcdB. The results of this study present copper ion-catalyzed oxidative detoxification of toxic proteins as a method highly suitable for the rapid production of safe, immunogenic and irreversible toxoid antigens for future vaccine development and may have the potential for replacing cross-linking reagents like formaldehyde.

Keywords: *Clostridioides difficile*, CDI vaccine**,** Reactive oxygen species, Metal-catalyzed oxidation, Toxoid

1. Introduction

C. difficile infection is the leading cause of healthcare-associated diarrhea and is responsible for around 453,000 incidences and 29,000 deaths every year in the United States alone [1]. More than 80% of CDI-related deaths occur in patients with age above 65 years leading to health care costs of approximately US$ 6 billion per year in the United States [2]. This spore-forming, gram-positive anaerobic bacterium gives rise to a spectrum of disease symptoms, ranging from mild diarrhea to pseudomembranous colitis, toxic megacolon, and death [3,4]. The primary cause of pathogenicity by *C. difficile* is due to its clostridial toxins, TcdA and TcdB [5], which are large proteins with a molecular weight of 308 kDa and 270 kDa, respectively, sharing structurally similar functional domains [6]. Both toxins are transferred into the host cell cytoplasm by receptor-mediated endocytosis where low pH in the endosome triggers conformational changes of the toxins activating the translocation of a catalytic domain across the membrane. Once inside the toxins inactivate Rho GTPases by attaching a glucose moiety to a catalytically important residue of the GTPase. This causes a degradation of the actin cytoskeleton leading to cell death [7]. Although there have been some contradicting reports of the individual potency and cytotoxic effects of each toxin [8–11] most *in vivo* studies suggest that they both contribute to disease during a natural infection [8,12].

The primary treatment of CDI consists of narrow-spectrum antibiotics such as metronidazole, vancomycin, and fidaxomicin [13]. However, non-responders to metronidazole and vancomycin have been reported [14,15]. After treatment of the patient´s first episode of CDI the risk of recurrence is 20-30% and no approved antimicrobial treatment exists that provides a lower probability of secondary CDI recurrence, which occurs in 40-60% of patients overcoming the first recurrence [16]. Recurrent CDI is likely a consequence of resident and long-lasting spores, reinfection, or the disruption of healthy microbiota due to the antibiotic treatment(s) [16,17]. The importance of a commensal gut

66 microbiota against recurrent CDI is supported by successful reports of fecal transplantations, with
67 disease resolution up to ca. 90% of patients [18,19].

68 Studies in both animals and humans have shown that vaccination with detoxified TcdA and
69 TcdB protects against CDI symptoms [20–23]. Thus, neutralization of TcdA and TcdB by toxin-
70 specific antibodies is potentially an efficient method for preventing disease symptoms [24,25], and
71 several toxoid-based vaccine candidates have made it to clinical trials [26–28]. Conventional
72 detoxification methods such as cross-linking by formaldehyde have previously been used to detoxify
73 toxins for vaccine production [29–31]. For instance, formaldehyde is successfully used in licensed
74 toxoid-based vaccines against tetanus and diphtheria [32]. Unfortunately, formaldehyde-based
75 detoxification has several disadvantages including i) slow and time-consuming [29], ii) risk of toxic
76 reversibility over time [33,34], iii) inherent carcinogenicity and toxicity associated with formaldehyde
77 [35,36] and finally, iv) suboptimal immunogenicity in some vaccines due to intra- and intermolecular
78 cross-linked toxoids [37–39]. Thus, there is a need for identifying alternative approaches for rapid
79 formation of safe, stable and highly immunogenic toxoids for future vaccines.

80 Oxidizing agents including divalent metal ions [40] and H_2O_2 [41] have long been used as
81 antiseptics, disinfectants and for inactivation of virulence factors such as toxins [42]. Furthermore, it
82 has been shown that the reactive oxygen species (ROS) produced via a Fe^{3+}/H_2O_2/EDTA system
83 could effectively detoxify pertussis toxin. This method has produced a safe and irreversibly detoxified
84 pertussis toxoid [43,44], with higher epitope conservation than the formaldehyde-detoxified vaccine
85 [38]. Despite the widespread knowledge, ROSs are widely considered agents of irreversible damage
86 to biomolecules and tissues and the full advantage of these active oxygen species for contributing to
87 medical advances has not been realized fully. In this study, using pH-dependent conformational
88 modulation of TcdA and TcdB combined with a controlled copper ion-catalyzed protein oxidation

method developed by us previously [45,46], we describe an efficient, permanent and safe method for producing highly immunogenic toxoids of TcdA and TcdB.

2. Materials and Methods

2.1 Chemicals and reagents

Stabilizer-free 30% hydrogen peroxide (H_2O_2 30%) and copper(II)chloride dihydrate ($CuCl_2 \cdot 2 H_2O$), was obtained from Merck Chemicals GmbH (Darmstadt, Germany). Whereas, iron(III) sulfate ($Fe_2(SO_4)_3 \cdot 7 H_2O$), Trizma base, crystal violet solution and SYPRO orange dye was purchased from Sigma-Aldrich (St. Louis, MO, USA). Formaldehyde (4%, v/v) solution was obtained from VWR (Gliwice, Poland) and ethylenediaminetetraacetic acid disodium salt (2Na-EDTA) was obtained from BDH Ltd. (Poole, England). Monoclonal mouse anti-TcdA and anti-TcdB antibodies were purchased from tgcBIOMICS (Bingen, Germany). AP-conjugated goat anti-mouse IgG (H+L) was purchased from Dako A/S (Glostrup, Denmark). HRP-conjugated rabbit anti-mouse (H+L) was purchased from Southern Biotech (Birmingham, AL, USA). TMB PLUS2 was obtained from Kem-En-Tec Diagnostics A/S (Taastrup, Denmark). Dulbecco's Modified Eagle Medium (DMEM) was obtained from ThermoFisher (Waltham, MA, USA). Tryptone and Yeast Extract were obtained from Formedium (Norfolk, UK). Tryptone, yeast extract, mannitol (TYM) consists of 24 g/L tryptone, 12 g/L yeast extract, 10 g/L mannitol, 1 g/L glycerol where tryptone, yeast extract, sodium thioglycolate (TYS) consists of 30 g/L tryptone, 20 g/L yeast extract, 1 g/L sodium thioglycolate. HiTrap Q FF column (4 x 5 mL serially connected), MonoQ 10/100 GL column and HiPrep 16/60 Sephacryl S-300 column were purchased from GE Healthcare Life Sciences (Pittsburgh, PA, USA).

2.2 Purification of *C. difficile* TcdA and TcdB

TcdA and TcdB toxins from *C. difficile* Ribotype 027 (NCTC 13366) were purified using the dialysis bag method as described previously [47]. Briefly, an overnight anaerobic culture of *C. difficile* in TYM medium was inoculated (1%, v/v) into 2 L of sterile 0.9% saline in a dialysis bag suspended in 15 L of TYS. The media were pre-reduced with nitrogen and autoclaved before inoculation. Cultures were grown for 72 hours at 37 °C, centrifuged at 18.500 x *g* for 20 min at 4 °C and dialyzed using a Quattro 1000 Ultrafiltration/Diafiltration with a 50 kDa cut-off membrane in 50 mM Tris-HCl (pH 7.5). Separation of TcdA and TcdB from the dialyzed supernatants was achieved using a HiTrap Q FF anion-exchange column, integrated on a fast protein liquid chromatography (FPLC). The toxins were eluted with a linear 0 to 1 M NaCl gradient, with TcdA eluting at 150 - 200 mM NaCl and TcdB at 400 - 450 mM NaCl. Fractions were visualized on SDS-PAGE and protein sizes corresponding to either TcdA or TcdB were pooled and further purified using a HiPrep 16/60 Sephacryl S-300 size-exclusion column. In the final step, a high-resolution anion-exchange MonoQ 10/100 GL column was used.

2.3 Differential scanning fluorimetry (DSF)

Using a 96-well plate (MicroAmp, applied biosystems, USA), 2 µL of SYPRO Orange dye (62x concentrated stock) was mixed with 1.25 µM TcdA or 0.8 µM TcdB in individual pH-adjusted buffers to a final volume of 25 µL. The plate was centrifuged for 1 min at 2300 x *g* before placing it into the ABI 7500 Real-Time Polymerase Chain Reaction machine. The temperature gradient was set to run from 20 to 95 °C with an increase of 1 °C/min, as described previously [48]. The fluorescence signal was recorded and the obtained data were analyzed and processed on Graphpad Prism software version 8 (San Diego, CA, USA).

2.4 Circular dichroism (CD) spectroscopy

Secondary and tertiary structural changes in TcdA and TcdB were probed using far-UV (200−260 nm) and near-UV (250-320 nm) CD spectroscopy. A Jasco J-815 spectropolarimeter equipped with a Peltier-element-controlled thermostat was used for all studies. All CD measurements were performed with a spectral bandwidth of 2 nm and a scanning speed of 50 nm min^{-1}. Far-UV measurements were performed using a cell of 0.1-cm path length and near-UV measurements were performed using a cell of 1.0-cm path length. The temperature stability studies were performed by heating TcdA or TcdB to the desired temperature, incubating for 5 min before measuring the CD spectrum, followed by heating to the next temperature and measuring a new CD spectrum. The studies monitoring the secondary/tertiary structure of the toxins/toxoids after metal-catalyzed oxidation were measured at 25 °C. The final CD spectra were obtained by subtracting the spectrum of the sample buffer from the mean sample spectrum of two individual scans using Jasco Spectra Analysis software, with a Savitzky-Golay algorithm of convolution width 11 applied as described previously [45,46]. Molar ellipticity ([θ]) in units of mdeg cm^2 $dmol^{-1}$ was calculated as

$$[\theta] = \frac{\text{mdeg} \cdot M_w}{10 \cdot L \cdot c}$$

where *[θ]* is calculated molar ellipticity, *mdeg* is experimentally measured ellipticity in mdeg, M_w is protein molecular weight (g/mol), L is the optical path length (cm), c is the protein concentration (mg/ml).

2.5 Metal-catalyzed oxidation of TcdA and TcdB

Inactivation of TcdA and TcdB was achieved by Cu^{2+}/H_2O_2 mediated metal-catalyzed oxidation (MCO) as previously described [45,46]. Briefly, in a pilot experiment MCO reactions with varying Cu^{2+} (15, 30 and 37.5 μM) and H_2O_2 (50, 250, 500 and 1000 μM) concentrations were set to oxidatively modify TcdA (0.5 μM) at four pH values (4, 4.5, 5, 7.5) for 2 h at 37 °C and the MCO reaction was terminated by adding an optimized 2 mM EDTA [45,46] and incubation on ice (Supplementary Table S1). Protein concentrations were measured by direct absorbance at 280 nm using a NanoDrop ND-1000 spectrophotometer. All buffers consisted of 50 mM Tris with pH adjusted using acetic acid. From the pilot experiment, the best condition showing the highest levels of TcdA inactivation was further subjected to time-dependence trials at four-time points (30, 60, 90, 120 min) as shown in Supplementary Fig. S1. Around 3 - 4 μM of the toxin was mixed with pH-adjusted MCO components (toxin: Cu^{2+}: H_2O_2) in a molar ratio of 1:60:1000, which were the optimal conditions for the final preparation of the toxoids. The reaction mixtures were mixed gently and transferred to a 37 ºC heating block. Control samples were also prepared at each pH value without $CuCl_2$ and H_2O_2. Further control samples were prepared at pH 4.5 and 7.5 each containing one component of the reaction system (Supplementary Fig. S2 and S3). All samples were either analyzed immediately or after being stored a maximum of 2 h on ice.

2.6 *In vitro* cytotoxicity

Cell toxicity of native and MCO-detoxified TcdA and TcdB was tested using Vero cell culture ($5x10^4$ cells/ mL DMEM) [49]. After adding 150 μL Vero cell culture to each well in a 96-well microtiter plate the plates were incubated in a HeraCell 150i CO_2 incubator at 36.5 °C and 5% CO_2 for 24 h prior to cytotoxicity testing. Native toxin and/or MCO-detoxified samples (10 μL) were

177 added to the first well in each row, followed by serial dilution. After 48 h of incubation at 36.5 °C the
178 level of cell rounding was assessed by visual inspection using a microscope. To further verify the
179 visual assessment the plates were emptied for media and washed twice with 200 µL/well PBS buffer.
180 After washing, 200 µL/well (4%, v/v) formaldehyde was added and incubated at room temperature
181 for 10 min, followed by another washing step. Finally, the fixed cells inside the wells were stained
182 using 0.1% crystal violet (200 µL/well), placed at room temperature for 10 min and washed gently
183 with deionized water. Stained plates were photographed using a Bio-Rad Gel Doc Imager and
184 qualitatively inspected.

185

186 **2.7 SDS-PAGE and Western Blot analysis**

187 TcdA and TcdB samples were visualized by reducing SDS-PAGE using TGX Stain-free™
188 mini-protein gels (Bio-Rad, Hercules, CA, USA). Fifteen µL sample (0.5-1 µM/well) was mixed with
189 5 µL of 2 x Laemmli Sample Buffer (Bio-Rad, USA), and incubated for 20 min at room temperature.
190 Electrophoresis was carried out using TGS SDS Buffer (Bio-Rad, USA) for 30 min at 200 V, 500
191 mA. Bio-Rad Precision Plus Protein Standard (4 µL/well) was used as a molecular weight marker.

192 For Western Blot analysis, SDS-PAGE gel bands were transferred to a Trans-Blot Turbo 0.2
193 µm nitrocellulose membrane (Bio-Rad, USA) using electroblotting on a Bio-Rad Trans-Blot Turbo
194 Transfer System for 7 min at 25 V, 2.5 A. Subsequently, the nitrocellulose membrane was blocked
195 with 5% w/v skim milk/TBS buffer for 30 min at 37 °C with shaking, and thereafter washed 3x5 min.
196 in TBS at 37 °C with shaking. After washing, the membrane was incubated for 1 h at 37 °C with
197 mouse anti-TcdA or anti-TcdB antibodies diluted 1:100,000 in skim milk/TBS. Another washing step
198 was performed, where after the blots were incubated for 1 h at 37 °C with goat anti-mouse AP-
199 conjugated antibody diluted 1:1000 in skim milk/TBS, followed by a final washing step. For

visualization of antibody binding, SigmaFast BCIP/NBT tablets (Sigma-Aldrich, St. Louis, MO, USA) were used.

2.8 Stability study

Native and MCO-detoxified TcdA and TcdB samples were incubated at -20 °C, 4 °C and 25 °C for 26 or 28 days. Detoxified TcdA was kept at pH 4.5 during storage, whereas detoxified TcdB was adjusted to pH 7.5 for storage. Cytotoxicity was measured for all samples using Vero cells. Furthermore, secondary structure was analyzed for all samples before and after incubation at the various temperatures using far-UV CD at 200 – 260 nm.

2.9 Epitope recognition study

Polystyrene MaxiSorp microtiter plates (Nunc) were coated with 100 µl of either 1 µg/ml native or detoxified TcdA and TcdB, respectively, in 0.05 M Na_2CO_3, 0.05 M $NaHCO_3$ (pH 9.6) and incubated overnight at 5 °C. The next day, wells were blocked with 300 µl of 1% (w/v) BSA in PBS-0.05% (v/v) Tween (pH 7.4) and incubated for 2 h at 37 °C. One hundred µl of serially diluted monoclonal antibody (1:4 in 1% BSA in PBS-0.05% Tween) was added to each well in triplicates and incubated for 1 h at 37 °C. HRP-conjugated rabbit anti-mouse IgG diluted 1:5000 in 100 µL of 1% BSA in PBS-0.05% Tween was added to each well, followed by incubation for 1 h at 37 °C. Antibody binding was visualized by the addition of 100 µL TMB PLUS2 substrate and incubation at room temperature for 15 min, and the reaction was stopped by adding 50 µL of 0.2 M H_2SO_4. Absorbance was measured at 450 nm using a POLARstar OPTIMA microplate reader (BMG

221 laboratories). Plates were washed 5 times with 250 µL washing buffer (PBS-0.05% Tween 20)
222 between each step.

223

224 **2.10 Toxoid preparation for mouse challenge study**

225 The MCO-detoxified vaccine was prepared by individually mixing 11.2 µM and 11.9 µM TcdA
226 and TcdB, respectively, with pH 4.5-adjusted MCO components in a molar ratio of 1:60:1000 for
227 toxin:Cu^{2+}:H_2O_2 and incubated at 37 ºC for 2 h. MCO reactions were terminated by adding EDTA to
228 a final concentration of 2 mM, adjusting pH to 7.5 and transferring the tubes to 4 ºC. The
229 formaldehyde-detoxified vaccine was prepared by individually dialyzing 5.5 µM TcdA and TcdB into
230 0.1 M phosphate buffer, pH 7±0.2 using 30 kDa cut-off centrifugal filters (Amicon). Then
231 formaldehyde was added to a final concentration of 0.45% (v/v) and the samples incubated at room
232 temperature (25 ºC) for 7 days. Samples were then dialyzed against 0.1 M phosphate, 0.1 M NaCl,
233 pH 7±0.2 using 30 kDa cut-off centrifugal filters at 4 ºC to remove the formaldehyde. Formaldehyde
234 was added to a final concentration of 0.016% (v/v) after dialysis to prevent the reversion of toxicity,
235 and samples were stored at 4 ºC. Each individual toxin from the MCO- and formaldehyde-detoxified
236 samples were diluted to 0.2 mg/ml and mixed with aluminium hydroxide (Alhydrogel®) to a final
237 concentration of 2 mg/ml and incubated for 24 h at 4 ºC shaking at 250 rpm. The next day, aluminium
238 hydroxide-adsorbed TcdA and TcdB samples were mixed in equal ratios of TcdA and TcdB, in a final
239 vaccine formulation consisting of 0.1 mg/ml TcdA, 0.1 mg/ml TcdB and 2 mg/ml aluminium
240 hydroxide. Each vaccine dose of 50 µL contained 5 µg TcdA and 5 µg TcdB, detoxified with either
241 MCO or formaldehyde.

242

2.11 Mouse challenge model of CDI

The experimental protocol for this animal study was approved by The Danish Experimental Animal Inspectorate (No. 2018-15-0201-01387), and all applicable national guidelines for the care and use of animals were followed. Female C57BL/6J-OlaHsd mice, 8- to -10 weeks old and weighing approximately 18 g (Envigo, UK) were housed in three groups of 8 per cage under similar conditions. Food (Teklad 2916 Global 16% protein rodent diet, Envigo), bedding (Tapvei aspen), nesting material (Enviro-dri), cage enrichments (cardboard house, dried corn, peanuts, sunseed – given twice a week) were all irradiated before use. Food and water were given ad libitum. Housing was a Type III cage and washed prior to use. The experimental model used in this study was based on the model developed by Chen *et al.* [50] and Erikstrup *et al.* [51]. Mice were immunized with a 50 µL vaccine dose two times, on days 0 and 21 by intramuscular injection. The animals received either a formulation with MCO-detoxified vaccine (n = 8), formaldehyde-detoxified vaccine (n = 8) or an aluminium hydroxide (mock) control (n = 8). Blood samples were collected on days 0, 21, 49 and 60. In order to establish CDI, the normal enteric microbiota was disrupted by pretreating the mice with an antimicrobial mixture in the drinking water, for 3 days starting on day 50, containing kanamycin (40 mg/kg), gentamycin (3.5 mg/kg), colistin (4.2 mg/kg), metronidazole (21.5 mg/kg) and vancomycin (4.5 mg/kg). The concentration of the antimicrobial mixture was calculated based on the average weight of the mice and their expected water consumption. On day 53, the mice were switched back to regular drinking water and on day 55 all mice were intraperitoneally injected with a 200 µL single dose of clindamycin (25 mg/kg). On day 56, all mice were challenged with 250 µL of 0.3 x 10^7 colony-forming units (CFU) of vegetative *C. difficile* Ribotype 027 (NCTC 13366) by oral gavage. The mice were monitored for signs of disease (diarrhea, wet tail, weight loss) and death. A clinical scoring system based on activity level, weight loss, changed breathing, appearance of eyes and fur was used at least 5 times per day with strict criteria to euthanize moribund animals.

2.12 Serum IgG measurements by ELISA

Polystyrene MaxiSorp microtiter plates (Nunc, Denmark) were coated with 100 µl of either 1 µg/ml TcdA or TcdB in 0.05 M Na_2CO_3, 0.05 M $NaHCO_3$ pH 9.6 and incubated overnight at 5 °C. The next day, wells were blocked with 300 µl of 1% BSA in PBS pH 7.4 and incubated for 2 h at 37 °C. Each mouse serum was 3-fold serially diluted in 0.5% BSA-PBS and 100 µl was added to each well in triplicates and incubated for 1 h at 37 °C. HRP-conjugated rabbit anti-mouse IgG diluted 1:5000 in 100 µL 0.5% BSA-PBS was added to each well, followed by incubation for 1 h at 37 °C. The antibody binding was visualized by the addition of 100 µL TMB PLUS2 substrate and incubation at room temperature up to 10 min, and the reaction was stopped by adding 100 µL of 0.2 M H_2SO_4. Absorbance was measured at 450 nm using a POLARstar OPTIMA microplate reader (BMG laboratories). Plates were washed 5 times with 250 µL washing buffer (PBS, pH 7.4, containing 0.05% (v/v) Tween 20) between each step.

2.13 Toxin Neutralization Assay (TNA)

One hundred µL cell culture in DMEM was added to each well in a 96-well microtiter plate and incubated in a HeraCell 150i CO_2 incubator at 36.5 °C and 5% CO_2 for 24 h prior to testing. Titrations of TcdA and TcdB were tested for the toxin concentration causing 50% rounding of cells (TC_{50}) prior to TNA studies. A concentration of 4 x TC_{50} for TcdA (4 ng/ml) or TcdB (7 ρg/ml) was pre-incubated with a 2-fold serial dilution of sera from immunized animals for 90 min at 36.5 °C with 5% CO_2 prior to their addition to the cell culture. One hundred µL of toxin-sera mixture was added to each well containing 100 µL cell culture and the plates were incubated for 48 h at 36.5 °C with 5% CO_2. Cell rounding was inspected as described in the "*In vitro* cytotoxicity" paragraph.

2.14 Statistical analysis

DSF curves and all ELISA titers are presented as the mean of three individual replicates. All statistical analysis of the data was performed using GraphPad Prism 8 software. Unpaired Student's t-test was used to calculate p-values for IgG titers and mean relative weights, whereas Mantel-Cox log-rank test was conducted on the Kaplan-Meier survival curves. P-values < 0.05 was taken as significant.

3. Results

3.1 Native expression of TcdA and TcdB

Native forms of TcdA and TcdB were expressed using the *C. difficile* Ribotype 027 strain (NCTC 13366). Brain Heart Infusion (BHI) broth is generally used as a growth medium for *C. difficile* for native toxin expression [52,53], however, we found that using a growth medium containing tryptone, yeast extract and sodium thioglycolate (TYS) produced a higher yield of toxins compared to BHI (Supplementary Fig. S4). After 72 h of incubation at 37 °C under anaerobic conditions, the toxins were purified from the culture supernatant using FPLC chromatography. Purified TcdA and TcdB were evaluated by SDS-PAGE and western blot (WB) analysis in a neutral and acidic buffer respectively, to evaluate if the toxins were degraded under the harsher acidic conditions (Fig. 1A and 1B). SDS-PAGE and antibody recognition of the neutral and acidic stored toxins confirmed the presence of intact protein bands for both TcdA and TcdB.

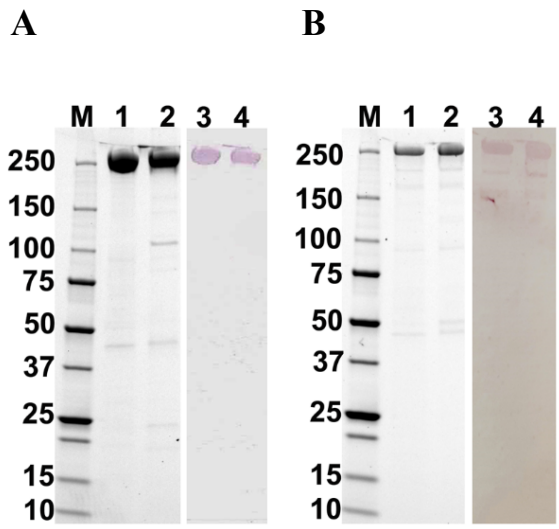

Figure 1. SDS-PAGE and WB analysis of native TcdA and TcdB. TcdA (0.9 µM) and TcdB (0.6 µM) were stored for 2 hours at 37 °C in either neutral or acidic conditions prior to analysis. **A:** TcdA samples; lane M: molecular weight markers (kDa), lane 1: TcdA in pH 7.5 (protein stain), lane 2: TcdA in pH 4.5 (protein stain), lane 3: TcdA in pH 7.5 (western), lane 4: TcdA in pH 4.5 (western). **B:** TcdB samples; lane M: molecular weight markers (kDa), lane 1: TcdB in pH 7.5 (protein stain), lane 2: TcdB in pH 4.5 (protein stain), lane 3: TcdB in pH 7.5 (western), lane 4: TcdB in pH 4.5 (western).

311

312 **3.2 Temperature stability of native purified TcdA and TcdB**

313 The changes in the secondary structure of TcdA (Fig. 2A) and TcdB (Fig. 2B) with increasing
314 temperature (25 to 80 °C) were monitored using circular dichroism (CD) in the 200 - 260 nm region.
315 TcdA shows well-defined far-UV CD spectra from 25 °C to 37 °C with similar spectral shapes and
316 two negative peaks at 208 and 218 nm (Fig. 2A). This indicates that the secondary structure of TcdA
317 is stable and largely intact during heating to 37 °C. However, at 45 °C and 50 °C the spectra show a
318 slight change in the 208 nm region with a beginning loss of the negative peak at 208 nm. By further
319 heating to 60 °C, the loss of this characteristic peak is more severe, which is seen by the complete
320 loss of the negative peak at 208 nm, indicating the unfolding of secondary protein structure. Heating
321 TcdA to 70 °C and then to 80 °C, the far-UV CD spectra have now completely lost any well-defined
322 shape and the intensity of the CD spectra are significantly reduced overall, indicating denaturation of

TcdA. TcdB also shows a well-defined far-UV CD spectrum during heating from 25 °C to 37 °C with no significant changes in the spectrum, and the presence of two negative peaks at 208 nm and 218 nm (Fig. 2B). At 45 °C there is a slight increase in the intensity of the negative peak at 218 nm, showing the beginning of minor structural changes at this temperature. However, TcdB does not seem to show significant spectral changes in the 208 nm region at 45 °C, unlike what is seen for TcdA (Fig. 2A), instead there are slight changes in the 218 nm region. Further heating to 50 °C induces significant changes in the secondary structure, which is seen by a more profound increase in the negative peak at 218 nm. This trend continues and increases during further heating to 60 °C and 70 °C, but at 80 °C the far-UV CD spectrum has changed drastically and completely lost the two negative peaks. At 80 °C, the CD spectrum shows a sharp rounded shape with a minimum of around 216 nm, and a significant increase is seen in the spectral intensity compared to the initial spectrum before heating.

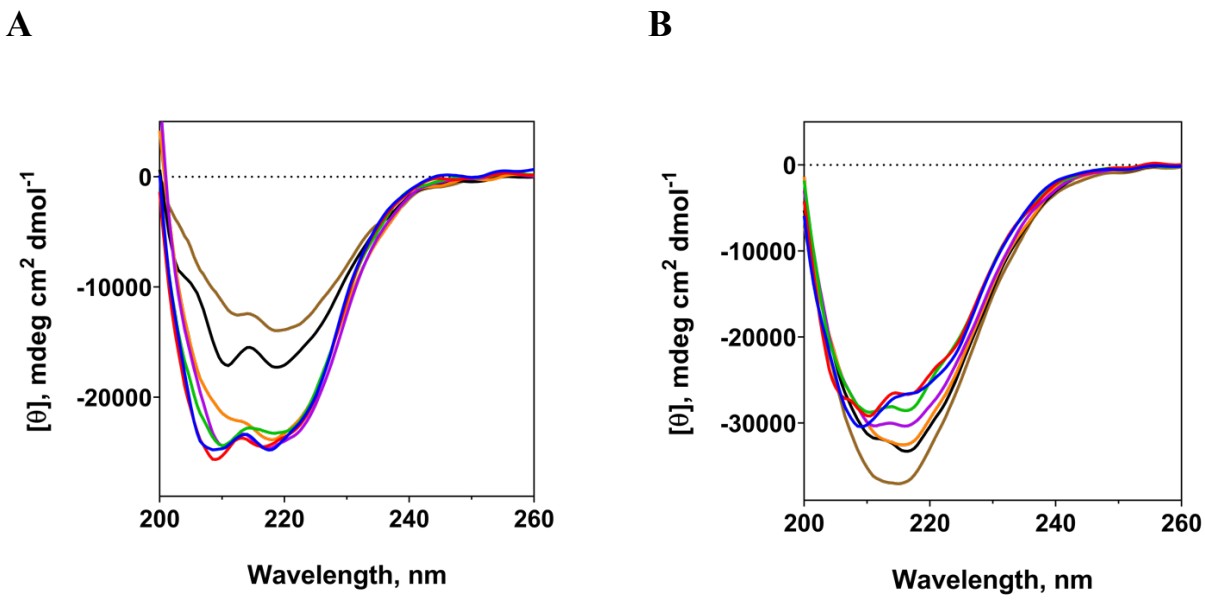

Figure 2. Effect of temperature on the secondary structure of TcdA and TcdB. Circular dichroism analysis of TcdA and TcdB, showing the change in the secondary structure during heating. The samples are kept for 5 min at each temperature before measurement, and the measurements are cumulative. **A:** 0.65 µM TcdA, **B:** 0.75 µM TcdB. Blue: 25°C, red: 37°C, green: 45°C, purple: 50°C, orange: 60°C, black: 70°C, brown: 80°C.

3.3 pH-induced thermostability changes

Differential Scanning Fluorimetry (DSF) analysis was performed on TcdA (Fig. 3A) and TcdB (Fig. 3B), in temperature ranges from 25 to 95 °C with an increase of 1°C/min. Both toxins were tested at five different pH conditions, ranging from pH 4 to 7.5, and the resulting melting temperatures (T_m) are listed in (Fig. 3C). The melting temperature (T_m) for TcdA at pH 7.5 is 51.5 °C, which is in alignment with the result obtained from the far-UV CD spectrum (Fig. 2A) showing initiation of unfolding at 45 - 50 °C. When lowering the pH to 6 and 5 respectively, no significant changes in the T_m values are observed. We only see a slight decrease of 1 °C which lowers the T_m of TcdA in pH 6 and 5 to 50.5 °C, indicating that the thermal stability of TcdA is not significantly affected in the pH range of 7.5 to 5. However, by lowering the pH further to acidic levels of 4.5 and 4, a significant decrease can be seen in the T_m for TcdA. At pH 4.5 there is a 4.5 °C decrease in the T_m reaching 47 °C, and at pH 4 the decrease in T_m is as high as 9 °C reaching a melting temperature of only 42.5 °C. TcdB has a slightly lower melting temperature at neutral pH than TcdA, with a T_m of 49 °C. This also correlates with the data from the far-UV CD spectra (Fig. 2B), where the structural changes of TcdB at 50 °C are more significant than for TcdA (Fig. 2A) confirming that TcdB has a lower melting temperature. At pH 6 the T_m is 47.5 °C, showing that TcdB is relatively stable when lowering the pH from 7.5 to 6, but not as stable as TcdA. However, when lowering the pH further to 5, there is a significant decrease in the T_m to 39 °C, which is much lower than the T_m of TcdA at pH 5. When the pH is lowered to 4.5 the T_m of TcdB is further decreased by 7 °C reaching 32 °C. At pH 4, the T_m cannot be calculated as the melting curve had no visible transition phase during heating. From the DSF analysis (Fig. 3A and 3B), it is clear that at acidic pH around 4.5, TcdA and TcdB have lower melting temperatures than at neutral pH.

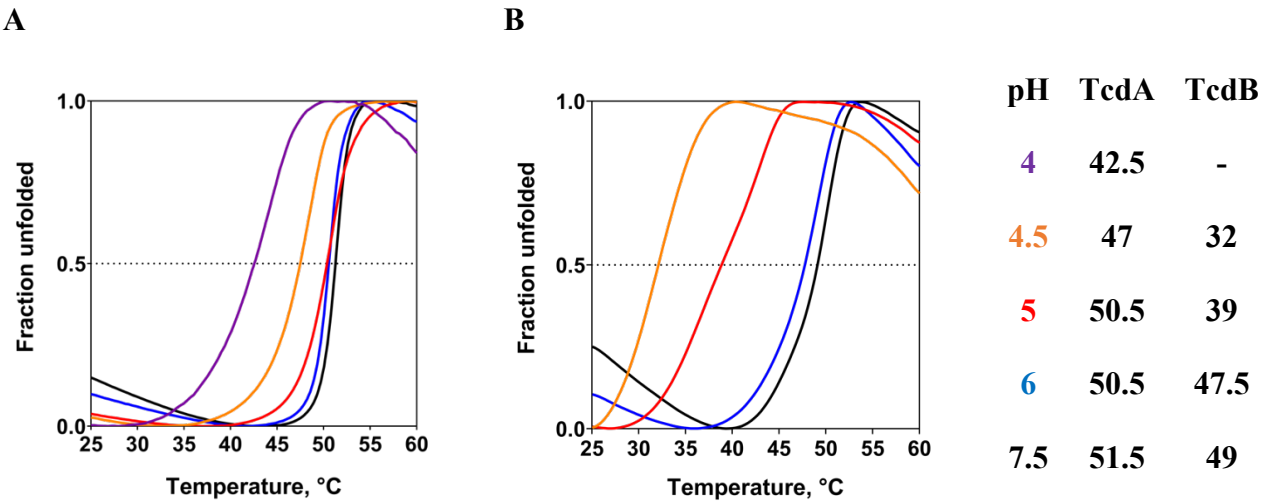

Figure 3. The effect of pH on the thermal stability of TcdA and TcdB. DSF was conducted using real-time PCR with a temperature gradient from 20 to 95 °C with an increase of 1°C/min (only 25 to 60 °C is shown). **A:** Each well contained 1.25 µM of TcdA, pH-adjusted buffer, and 2 µl of SYPRO orange dye (from 62x concentrated stock) in a final volume of 25 µl. **B:** Each well contained 0.8 µM of TcdB, pH-adjusted buffer, and 2 µl of SYPRO orange dye (from 62x concentrated stock) in a final volume of 25 µl. Black: 50 mM Tris-HCl pH 7.5, blue: 50 mM Na-citrate pH 6, red: 50 mM Na-acetate pH 5, orange: 50 mM Na-acetate pH 4.5, purple: 50 mM Na-acetate pH 4. The melting temperatures (T_m) are given in °C on the right.

3.4 Metal-catalyzed oxidation of TcdA and TcdB

Different pH ranges and MCO components were tested in order to identify and optimize mild oxidative conditions for detoxification of TcdA and TcdB. A concentration of TcdA (0.5 µM) at 37 °C was kept constant in the reaction mixture, and MCO treatment was tested at different pH values (4, 4.5, 5 and 7.5). The MCO components were also varied; $CuCl_2$ (15 to 37.5 µM) and H_2O_2 (50 to 1000 µM) as shown in Supplementary Table S1. All conditions were evaluated by SDS-PAGE, western blot analysis and Vero cell cytotoxicity assay (data not shown). These studies led to the optimal values of the MCO reaction components, which were determined to be molar ratios of 1:60:1000 for TcdA:Cu^{2+}:H_2O_2, respectively, with a reaction pH of 4.5 and a concentration of TcdA of 0.5 µM. Then the optimal conditions such as molar ratios of oxidants, buffer and pH obtained on TcdA were transferred to TcdB in further studies. With this knowledge, we proceeded to test MCO

on TcdA at pH 4.5 and at 37 °C with a range of different metal ions. All MCO samples were tested for cytotoxicity (Supplementary Fig. S5) and the results are summarized in Table 1. Of all the tested metal ions only Cu^{2+}/H_2O_2 system was able to induce a significant inactivation of TcdA with our MCO method, resulting in 6 $\log_{10}$ reductions of cytotoxicity relative to native TcdA. A similar level of TcdB inactivation was also achieved using Cu^{2+}/H_2O_2 system at pH 4.5 and 37 °C. The Fe^{2+}/H_2O_2 system and Fe^{3+}/H_2O_2 systems were only capable of reducing the cytotoxicity by a negligible 50-fold and 7-fold, respectively. None of the other metal ions had any significant effect on the cytotoxicity of TcdA as seen in Table 1. All conditions were evaluated by SDS-PAGE, western blot analysis and Vero cell cytotoxicity assay. TcdA and TcdB after MCO treatment at the optimal conditions were tested by cytotoxicity assay to determine the extent of reduction of cytotoxicity, in comparison to corresponding control samples (Supplementary Fig. S6 and S7) and summarized in Table 2.

The MCO detoxification of TcdA and TcdB at neutral pH using Cu^{2+} did not affect the cytotoxicity, whereas the same treatment at pH 4.5 showed more than 6 $\log_{10}$ fold reduction of the cytotoxicity for both toxins. It was also tested whether the individual components of the MCO reaction, such as Cu^{2+}, H_2O_2 or the acidification in itself had any significant detoxifying effect on the toxins (Supplementary Fig. S3), but the results showed that only the specific combination of Cu^{2+}, H_2O_2, and acidic pH range (4.0 to 4.5) is able to produce highly detoxified TcdA and TcdB toxoids. Finally, we studied the effect of different temperatures (25 to 37 °C) and incubation times (30 to 120 min) on the efficacy of MCO inactivation (Supplementary Figs. S1 and S8). We found that the optimal temperature and incubation time for effective inactivation of TcdA and TcdB is 37 °C and 120 min respectively.

Table 1. Effect of various metal ions on the MCO detoxification of TcdA

Metal salt	Metal-ion	Fold reduction in cytotoxicity
$CuCl_2$	Cu^{2+}	> 1,000,000
$MgCl_2$	Mg^{2+}	7
$CoCl_2$	Co^{2+}	7
$MnCl_2$	Mn^{2+}	7
$Fe_2(SO_4)_3$	Fe^{3+}	7
$FeSO_4$	Fe^{2+}	50
$CaCl_2$	Ca^{2+}	7
LiCl	Li^{+}	7
$NiCl_2$	Ni^{2+}	7
$AgNO_3$	Ag^{+}	7

All MCO reactions were conducted at pH 4.5 and each sample consisted of TcdA (1.2 μM), a metal salt (72 μM) and H_2O_2 (1200 μM) which were incubated for 2 hours at 37 °C and measured for cytotoxicity on Vero cells (Fig. S5).

391

392

Table 2. Effect of Cu^{2+}-catalyzed oxidation on the cytotoxicity of TcdA and TcdB

Toxin	Final toxin concentration (μM)	pH	Molar ratios (Toxin:Cu^{2+}:H_2O_2)	Fold reduction in cytotoxicity
TcdA native	1.3	7.5	1:0:0	1
TcdA native	1.3	4.5	1:0:0	50
TcdA MCO-detoxified	1.3	4.5	1:60:1000	> 1,000,000
TcdA MCO-detoxified	1.3	7.5	1:60:1000	5
TcdB native	1.5	7.5	1:0:0	1
TcdB native	1.5	4.5	1:0:0	350
TcdB MCO-detoxified	1.5	4.5	1:60:1000	> 1,000,000
TcdB MCO-detoxified	1.5	7.5	1:60:1000	5

All MCO reactions were incubated for 2 hours at 37 °C and measured for cytotoxicity on Vero cells (Figs. S6 and S7).

393

394

395 **3.5 MCO-induced structural changes**

396 The secondary structure of native and MCO detoxified TcdA and TcdB was monitored by far-
397 UV CD in the 200 - 260 nm region. Differences are observed in the 200 - 220 nm region between
398 MCO-detoxified and active TcdA (Fig. 4A). There is a slight loss of overall CD spectrum intensity
399 after MCO treatment, and the characteristic negative peak at 208 nm is lost, indicating some changes
400 in the α-helical structure of TcdA after oxidation. The same trend is seen for TcdB with a loss of the
401 characteristic negative peak at 208 nm for the oxidized TcdB at pH 4.5 (Fig. 5A). The CD results

align with the DSF results, showing that the toxins are more prone to structural changes at pH 4.5 (Fig. 3A and 3B). However, as seen in Fig. 5A (red line), the CD spectrum of MCO-detoxified TcdB could be reversed to the native-like state by raising the pH to 7.5 after oxidation. Surprisingly, when adjusting the pH of MCO-detoxified TcdA to 7.5, as we did for TcdB, we saw a significant reduction of CD spectrum intensity, indicating a degree of precipitation caused by the pH change.

The tertiary structure of native and MCO-detoxified TcdA and TcdB were monitored by near-UV CD. The spectra for native and MCO-detoxified TcdA both show an overall similar shape with two negative peaks at 275 and 282 nm (Fig. 4B). The CD spectrum of MCO-detoxified TcdA, however, has lower CD signal intensity compared to native TcdA, which could indicate that changes of the aromatic residues have occurred or that the protein has slightly precipitated. The near-UV CD spectrum of MCO-detoxified TcdB was monitored after readjusting pH to 7.5. The CD spectrum shows a similar shape and finer features compared to native TcdB with two negative minima at 275 and 282 nm (Fig. 5B). Like TcdA, the MCO-detoxified TcdB CD spectrum has lower signal intensity compared to the native TcdB spectrum.

Furthermore, to separate low pH and oxidative modification in the spectral changes of the CD, we monitored far-UV CD (Supplementary Fig. S9) and near-UV (Supplementary Fig. S10) of TcdA continuously during the MCO reaction at pH 4.5. CD measurements were conducted every 3 min to follow the progression of spectral changes. Interestingly, in the far-UV CD we see that already in the first spectrum after initiating oxidation there is a change between native TcdA at pH 4.5 to the MCO-detoxified TcdA at pH 4.5, meaning that MCO immediately causes more changes to the secondary structure than pH 4.5 alone. TcdA at pH 4.5 and the MCO-detoxified TcdA at pH 4.5, both show a progression of spectral changes over time, however, the spectral changes happen faster and are more extensive for the MCO-detoxified TcdA compared to TcdA at pH 4.5. The spectral changes progress until reaching a plateau around the 15 min time point. Near-UV CD spectra were also monitored for

the MCO reaction, and here we see an immediate change in the spectrum during the very first minutes of the MCO reaction (Supplementary Fig. S10).

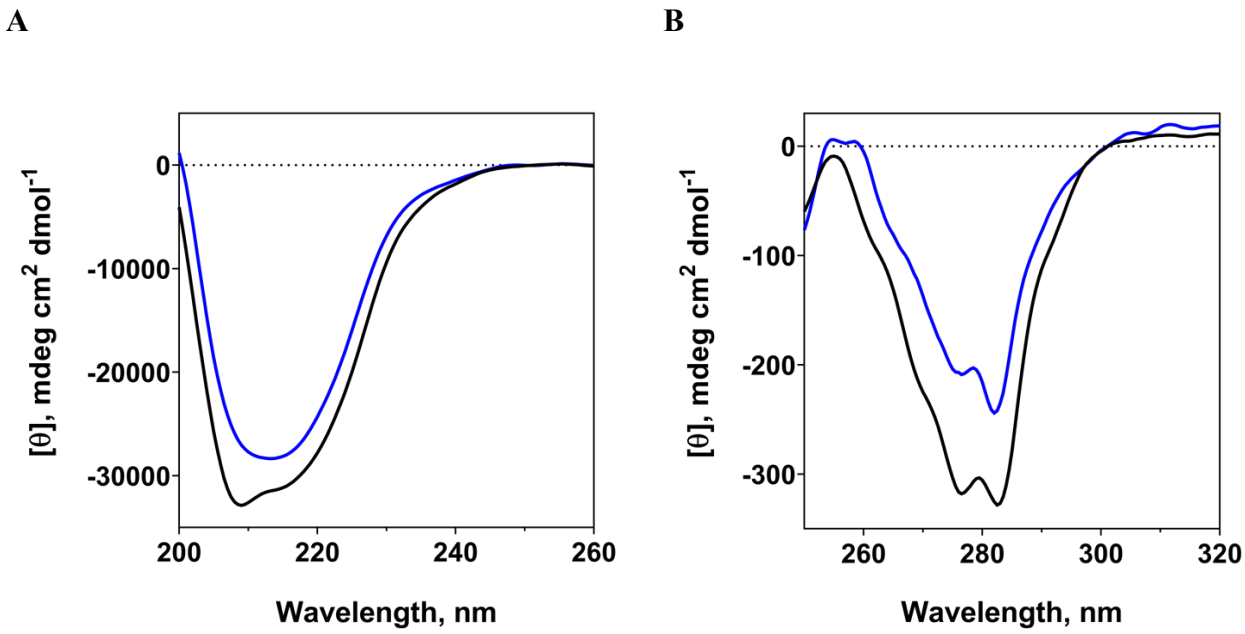

Figure 4. Circular dichroism analysis of native and MCO-detoxified TcdA. All samples are shown as an average of duplicate measurements with the buffer spectrum (blank) subtracted. **A:** Far-UV CD spectra ranging from 200 – 260 nm. The sample consisted of 1 µM TcdA. **B:** Near-UV CD spectra ranging from 250 – 320 nm. The sample consisted of 3.15 µM TcdA. Black: native TcdA pH 7.5, blue: MCO-detoxified TcdA pH 4.5.

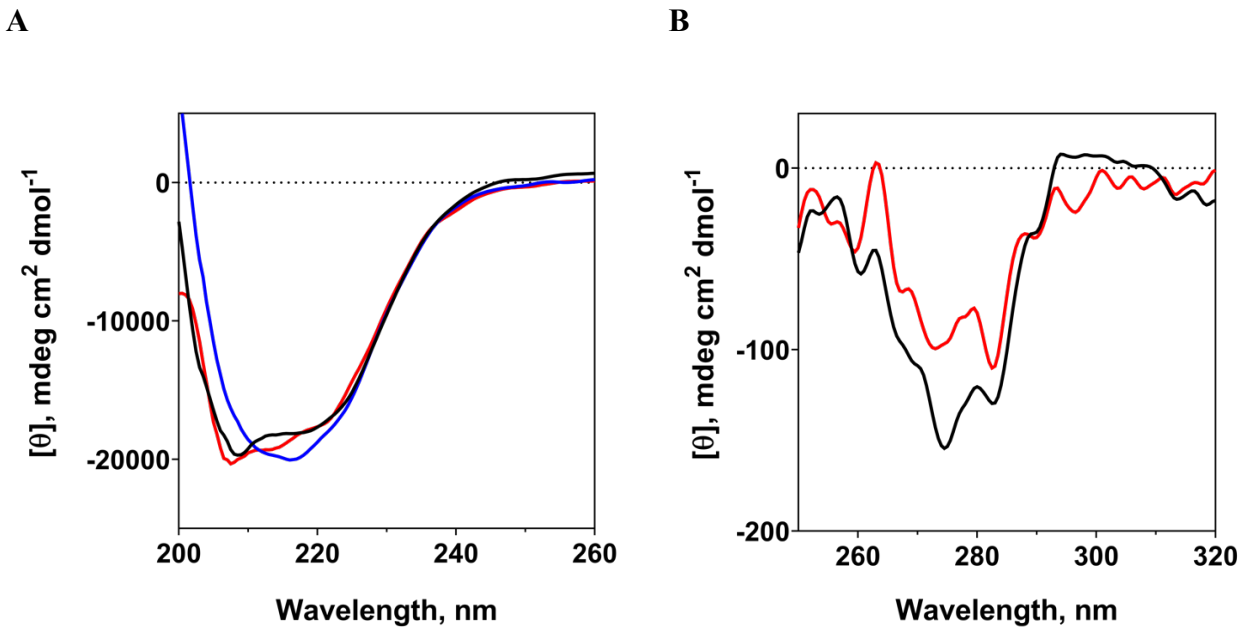

Figure 5. Circular dichroism analysis of native and MCO-detoxified TcdB. Far-UV CD samples are shown as an average of duplicate measurements with the buffer spectrum (blank) subtracted. Near-UV CD samples are shown as an average of 20 spectra with the buffer spectrum (blank) subtracted. **A:** Far-UV CD spectra ranging from 200 – 260 nm. The sample consisted of 0.75 µM TcdB. **B:** Near-UV CD spectra ranging from 250 – 320 nm. The sample consisted of 0.75 µM TcdB. Black: native TcdB pH 7.5, blue: MCO-detoxified TcdB pH 4.5, red: MCO-detoxified TcdB readjusted to pH 7.5.

429

430 **3.6 Epitope recognition after MCO detoxification**

431 The comparison between the binding of the mAbs to native and detoxified TcdA and TcdB are
432 shown in Table 3 and 4, respectively. The oxidation of TcdA slightly affected the epitope binding to
433 the six different mAbs. The ranges of mAb binding are between 12% and 79% with an average of
434 52%, relative to the binding of the mAbs to native TcdA. Formaldehyde detoxification has a
435 significantly more deleterious effect on the TcdA epitopes, as the binding capacity of the mAbs is
436 between 8% and 38% with an average of 21%. Detoxification of TcdB with either MCO or
437 formaldehyde follows a similar trend as TcdA, where MCO detoxification of TcdB leads to higher
438 epitope recognition by the mAbs compared to formaldehyde. The binding efficacy of the five mAbs

to MCO-detoxified TcdB is between 51% and 65% with an average of 57%, compared to binding to formaldehyde detoxified TcdB which is between 0% and 69% with an average of only 31%.

Table 3. Recognition of native and detoxified TcdA (TxdA) by monoclonal anti-TcdA antibodies

mAb (target)	Toxin		
	TcdA-native	**TcdA-MCO**	**TcdA-formaldehyde**
A-21 (C-terminal)	1.00	0.43	0.38
A-22 (C-terminal)	1.00	0.47	0.09
A-23 (C-terminal)	1.00	0.79	0.37
A-26 (C-terminal)	1.00	0.5	0.08
A-24 (N-terminal)	1.00	0.12	0.24
A-25 (N-terminal)	1.00	0.79	0.09

The recognition of MCO- or formaldehyde-detoxified TcdA by the mAbs is expressed as the ratio between the ELISA titer of the detoxified TcdA relative to the ELISA titer of native TcdA. The ELISA titer is defined as the endpoint titer, which is the highest dilution of mAb showing at least twice the A_{450} value of the blank wells. The ELISA titer of native TcdA is defined as 1.00. Formaldehyde-detoxification was conducted with 0.45% (v/v) formaldehyde, 30 mM lysine in 50 mM Tris pH 7.5 for 7 days at room temperature (25 °C).

Table 4. Recognition of native and detoxified TcdB by monoclonal anti-TcdB antibodies

mAb (target)	Toxin		
	TcdB-native	**TcdB-MCO**	**TcdB-formaldehyde**
B-72 (C-terminal)	1.00	0.65	0.37
B-75 (C-terminal)	1.00	0.57	0.1
B-76 (C-terminal)	1.00	0.57	0.38
B-71 (N-terminal)	1.00	0.51	0.69
B-74 (N-terminal)	1.00	0.55	0

The recognition of MCO or formaldehyde-detoxified TcdB by the mAbs is expressed as the ratio between the ELISA titer of the detoxified TcdB relative to the ELISA titer of native TcdB. The ELISA titer is defined as the endpoint titer, which is the highest dilution of mAb showing at least twice the A_{450} value of the blank wells. The ELISA titer of native TcdB is defined as 1.00. Formaldehyde-detoxification was conducted with 0.45% (v/v) formaldehyde, 30 mM lysine in 50 mM Tris pH 7.5 for 7 days at room temperature (25 °C).

3.7 Stability

Native and MCO-detoxified TcdA and TcdB were analyzed by far-UV CD and cytotoxicity testing after being stored for 26-28 days at either -20 °C, 4 °C, and 25 °C. Neither native nor MCO-detoxified TcdA shows significant changes in the shapes of the CD spectra at day 28 compared to day 0 when stored at any of the different temperatures (Fig. 6A-C). However, at all storage conditions, there is a significant reduction of the overall spectral intensity after 28 days for both native and MCO-

detoxified TcdA. TcdA samples (native and MCO-detoxified) show roughly the same level of spectral intensity loss when stored at -20 °C (Fig. 6A) and 4 °C (Fig. 6B) over 28 days, indicating that either precipitation and/or degradation is occurring equally for both. Surprisingly, native TcdA stored at 25 °C shows a more severe loss of CD spectrum intensity after 28 days, compared to the MCO-detoxified TcdA sample at 25 °C.

MCO-detoxified TcdB also shows well-preserved CD spectral features after either 26 or 28 days of storage (Fig. 6D-F). Similar to the TcdA samples, the CD spectra for both native and MCO-detoxified TcdB lose intensity overall during the storage period, likely caused by precipitation. Interestingly, after storage at 25 °C for 26 days the CD spectrum for native TcdB has significantly lower signal intensity compared to the MCO-detoxified TcdB CD spectrum, which is also seen for TcdA at 25 °C. None of the MCO-detoxified TcdA or TcdB samples show a reversal of cytotoxicity during the storage period at any of the storage conditions. A small decrease in cytotoxicity is observed during the storage period for both native and MCO- detoxified TcdA and TcdB, likely due to protein precipitation as mentioned above.

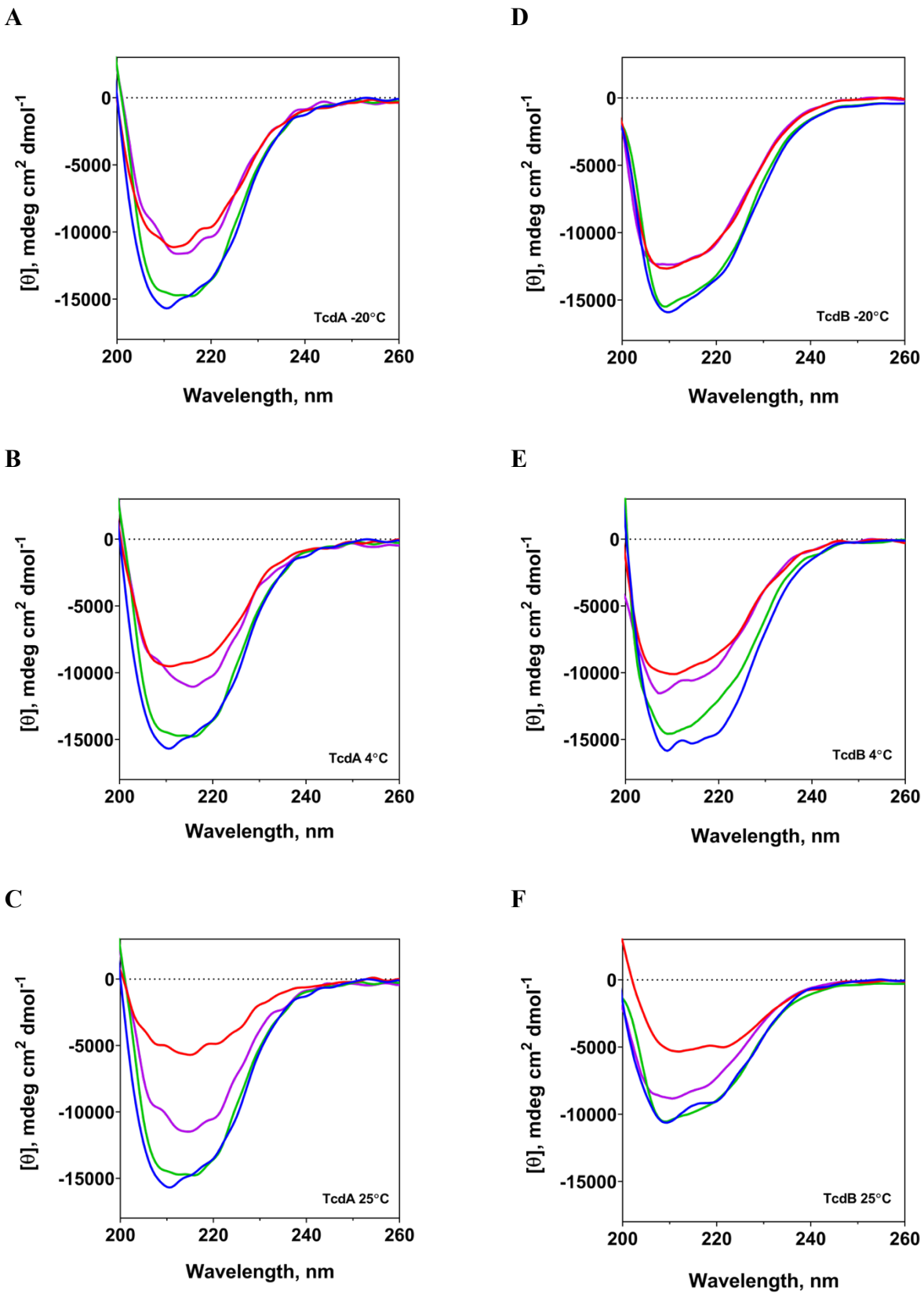

Figure 6. Long-term stability of native and MCO-detoxified TcdA and TcdB

Samples were analyzed using far-UV CD (200 – 260 nm) on day 0 and again on either day 26 or 28 after storage at different temperatures. **A:** 0.6 μM TcdA stored at -20 °C. **B:** 0.6 μM TcdA stored at 4 °C. **C:** 0.6 μM TcdA stored at 25 °C. Blue: native TcdA day 0, red: native TcdA day 28, green: MCO-detoxified TcdA day 0, purple: MCO-detoxified TcdA day 28. **D:** 0.7 μM TcdB stored at -20 °C. **E:** 0.7 μM TcdB stored at 4 °C. **F:** 0.7 μM TcdB stored at 25 °C. Blue: native TcdB day 0, red: native TcdB day 26/28, green: MCO-detoxified TcdB day 0, purple: MCO-detoxified TcdB day 26/28.

3.8 Immunogenicity and protective efficacy

Both vaccinated groups showed no visible side effects from the vaccine injections. No swelling around the injection site and no change in either weight or temperature. The MCO-detoxified vaccine and the formaldehyde-detoxified vaccine both fully protected against the oral challenge given on day 56, and all mice survived (Fig. 7A) while showing no signs of CDI disease symptoms such as diarrhea or weight loss (Fig. 7B). On the other hand, the unvaccinated control mice all exhibited CDI symptoms and three out of the eight mice were moribund and had to be euthanized within 3 days post-challenge.

To assess the development of toxin-specific IgG and neutralizing antibody responses in mice, sera samples were collected on days 0, 21, 49 and 60 after the primary immunization, and analyzed for levels of antibodies against native TcdA and TcdB, respectively, by ELISA and TNA. Immunization with both MCO- and formaldehyde-detoxified vaccine formulation elicited substantial anti-TcdA and anti-TcdB IgG responses, whereas control mice with mock injections had no detectable levels of antibodies in their sera (Fig. 7C and 7D). At day 60, mice immunized with the MCO-detoxified vaccine had mean anti-TcdA and anti-TcdB EC_{50} titers of around 4 $\log_{10}$, whereas the formaldehyde-detoxified vaccine-elicited mean anti-TcdA and anti-TcdB EC_{50} titers of around 4.2 $\log_{10}$ and 4.17 $\log_{10}$ respectively. There is no significant statistical difference between the mean anti-TcdA and TcdB EC_{50} titers induced by the MCO- and formaldehyde-detoxified vaccines, respectively. The same serum samples were tested for toxin neutralizing activity on Vero cells, where

native TcdA or TcdB were pre-incubated with serial dilutions of pooled sera for 90 min and added to cells. The MCO- detoxified vaccine was less efficient at eliciting neutralizing antibodies against TcdA compared to the formaldehyde-detoxified vaccine, with mean anti-TcdA neutralization titers at day 60 of around 3100 and 7300 respectively (Fig. 7E). We could not detect any anti-TcdB neutralizing antibodies in the sera of mice immunized with the MCO-detoxified vaccine, whereas the formaldehyde-detoxified vaccine was able to elicit a low mean anti-TcdB neutralization titer of around 600 at day 49 (Fig. 7F).

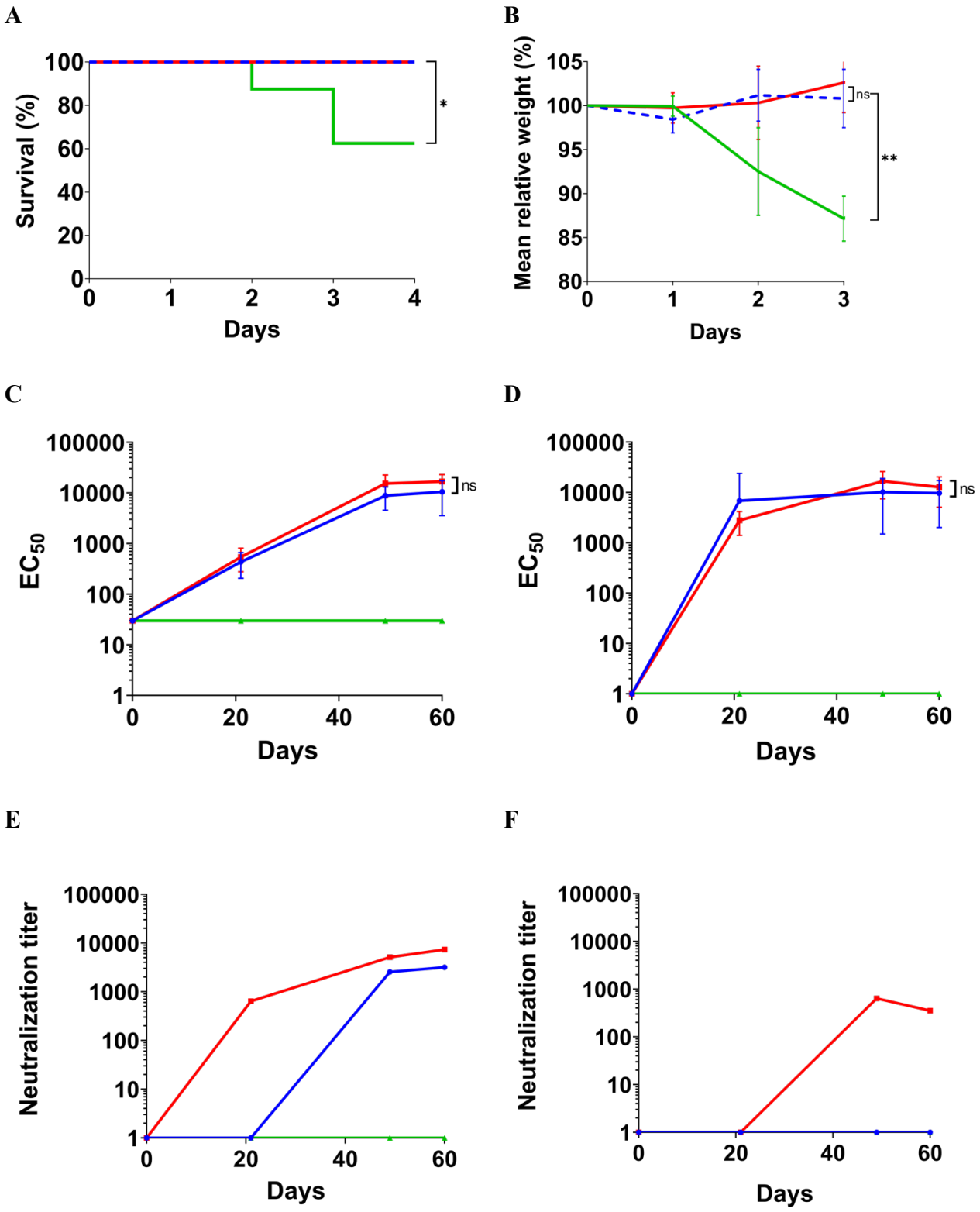

Figure 7. Survival and antibody response of vaccinated mice

Mice were immunized with either MCO-detoxified vaccine (blue), formaldehyde-treated vaccine (red) or an adjuvant control (green) before being challenged with *C. difficile* (n = 8 for all groups). Sera from days 0, 21, 49 and 60 were tested for anti-TcdA and anti-TcdB IgG titers by ELISA and neutralizing antibodies by TNA. For ELISA, a four-

parameter logistic curve was fitted to each serum sample by plotting the absorbance at 450 nm as a function of the serum dilution. **A:** Kaplan-Meier survival curve, with day 0 representing the day of *C. difficile* challenge. Statistical analysis of survival curves was performed using Mantel-Cox log-rank test ($p = 0.034$). **B:** Mean relative weight graph, where the relative weight of each mouse is based on its weight on the day of the challenge. Unpaired Student's t-test was used to compared weight curves. * = $p<0.05$, ** = $p<0.01$, *** = $p<0.001$, ns = no significant difference. **C:** Anti-TcdA IgG titers are shown as EC_{50} values, representing the serum dilution where the anti-TcdA response is reduced by 50%. Unpaired Student's t-test was used to compare EC_{50} values at day 60 ($p = 0.079$). **D:** Anti-TcdB IgG titers are shown as EC_{50} values, representing the serum dilution where the anti-TcdB response is reduced by 50%. Unpaired Student's t-test was used to compare EC_{50} values at day 60 ($p = 0.44$). **E:** Pooled sera were tested for anti-TcdA neutralization titers, which represents the highest dilution of sera where there is at least 50% cell survival after 48 h of adding the toxin-sera mixture. **F:** Pooled samples were tested for anti-TcdB neutralization titers, which represents the highest dilution of sera where there is at least 50% cell survival after 48 h of adding the toxin-sera mixture.

4. Discussion

In this study, a mild MCO condition is used as an efficient method to detoxify TcdA and TcdB without altering structural epitopes. MCO detoxification of TcdA and TcdB most likely occurs when metal ions, typically Cu^{2+}, Fe^{2+} or Fe^{3+}, interact with exposed functional sites on native TcdA and TcdB. The oxidizing species produced by reaction of copper with H_2O_2 remains contentious. However, in our previous studies [45,46] we have shown that Cu^{2+} and H_2O_2 mediate radical production and could lead to alterations in structure and function of the target proteins. The mechanism for the radical production in the presence of Cu^{2+} and in the absence of any reductant is suggested to be as following:

$$Cu^{2+} + H_2O_2 \rightarrow Cu^{+} + O_2^{-\bullet} + 2H^{+} \quad (1)$$

$$Cu^{2+} + O_2^{-\bullet} \rightarrow Cu^{+} + O_2 \quad (2)$$

$$Cu^{+} + H_2O_2 \rightarrow Cu^{2+} + HO^{-} + HO^{\bullet} \quad (3)$$

Hence the reduction of Cu^{2+} to Cu^{+} can take place by either H_2O_2 (reaction 1) or by superoxide radical anions (reaction 2). Furthermore, the reduced Cu^{+} (cuprous ions) could initiate a Fenton-like reaction with surplus H_2O_2 (reaction 3). This reaction could generate Cu^{2+}-$HO^{\bullet}$ or its ionized

513 equivalent, Cu^{2+}-$O^{\bullet}$, as suggested by [54]. Since we have not examined the type of radical produced
514 by the Cu^{2+}/ H_2O_2 reaction in this study, it is possible that other active species might be produced and
515 involved in the radical mediated reactions [55]. Hydroxyl radicals and other active species will react
516 almost instantaneously with amino acid side-chains near the interaction site. For this reason, the MCO
517 can be very protein specific depending on specific metal ion interactions sites in the protein as we
518 have seen for TcdA and TcdB in this study.

519

520 **4.1 Temperature-induced unfolding of TcdA and TcdB**

521 The temperature study was performed to determine the structural changes in the toxins during
522 increasing temperatures, and thereby determine the highest temperature we could use during the
523 inactivation reaction without altering their structure. The far-UV CD spectroscopy during increasing
524 temperatures show the presence of the characteristic double minima at 208 and 218 nm for TcdA
525 (Fig. 2A) and TcdB (Fig. 2B) at 25 °C and 37°C, indicating that the toxins possess a well-defined
526 secondary structure. The observed far-UV CD spectra can be explained by the diverse multi-domain
527 structure of the toxins, where each domain has a unique contribution [56,57]. The diverse secondary
528 structure composition is also confirmed from the crystal structures of TcdA [58] and TcdB [59]. The
529 effect of heating on the secondary structure of TcdA and TcdB is very different. Even though both
530 toxins are losing their characteristic and well-defined far-UV CD spectra at temperatures higher than
531 45 °C, the progression of this change is different. The spectral curve for TcdA displays a progressing
532 decrease in molar ellipticity during heating (Fig. 2A), indicating a shift towards more disordered
533 structure and unfolding of the α-helical and β-sheet structures [57,60]. In contrast, the spectral curve
534 for TcdB increases in molar ellipticity and instead progresses into a sharper negative minimum at 216
535 nm during heating (Fig. 2B), which could indicate an increase in β-sheet content [56]. These results

suggest that thermal denaturation of TcdA and TcdB have different unfolding patterns, in which TcdA unfolds and loses both its α-helical and β-sheet structure, whereas TcdB loses α-helical structure and gains a significant amount of new β-sheet structure. This indicates that TcdB likely aggregates at higher temperatures leading to intermolecular β-sheet interactions as shown for TcdB in a previous study [57] and also for other proteins [61–63]. Furthermore, the effects of thermal denaturation on TcdA and TcdB is an irreversible process, as cooling the toxins from 50 °C back to 25 °C had no effect on restoring their native-like CD spectra, which has also been reported previously by another group [57]. Temperatures between 25 °C and 37 °C were concluded to be favorable for detoxification studies, as the toxins were both structurally unmodified until at least 37 °C, while at 45 °C changes in their secondary structures started to occur.

4.2 TcdB is more sensitive to acidic pH changes than TcdA

The effect of pH on the thermostability of both toxins were tested by DSF analysis and suggests that the two toxins have quite different pH sensitivity. TcdA is slightly more heat resistant than TcdB at neutral pH with a T_m of 51.5 °C compared to 49 °C for TcdB. Furthermore, T_m for TcdA in the native folded state is up to 50 ºC in the pH range between 5 and 7.5 (Fig. 3A), whereas TcdB in the native folded state is up to 47 ºC only between pH 6 and 7.5 (Fig. 3B). These values are consistent with previous studies where Tam *et al.* [64] found a T_m of 49 °C for TcdB and Salnikova *et al.* [57] found T_m values of 52 °C and 47 °C for TcdA and TcdB respectively. However, in acidic conditions at pH 4.5, there is a dramatic difference between the folded state of the toxins. TcdA is partially unfolded around 47 °C, and TcdB is partially unfolded at only 32 °C. This is physiologically relevant, as pH 4.5 mimics the environment in the endosomes, and it is known that structural changes occur for both TcdA [65] and TcdB [59,66] when the pH environment in the endosome is lowered. The T_m

559 changes we see at pH 4.5 in the DSF analysis is, therefore, a result of the toxins' natural response to
560 acidification, where a structural change occurs to activate translocation across the endosomal
561 membrane [66–68]. TcdB seems to be much more affected by the acidic conditions, as it partially
562 unfolds at a much lower temperature than TcdA. At pH 4, the high initial fluorescence signal and lack
563 of transition phase in the DSF analysis of TcdB, suggests that the toxin is likely unfolded and/or
564 aggregated at lower temperatures [48]. This confirms that acidic conditions (pH 4 and 4.5) have a
565 significant effect on the unfolding behavior of both toxins, with TcdB being more sensitive to low
566 pH than TcdA.

567

568 **4.3 Acidification induced open conformation and Cu^{2+} catalyzed oxidation of TcdA and TcdB**

569 It is our hypothesis that partially exposed toxic regions of the TcdA and TcdB would allow
570 maximum accessibility to the produced ROS and thereby inactivation of TcdA and TcdB. Several
571 strategies (see Materials and Methods) to unfold and inactivate were investigated. However, at
572 neutral pH we did not observe any significant reduction in cytotoxicity albeit loss of protein band
573 intensity on SDS-PAGE was often observed. Thus, we turned our focus on the inherent structural
574 plasticity of the toxins at acidic pH. Our results from the CD (Fig. 2A and 2B) and DSF (Fig. 3A
575 and 3B) in combination with known literature [59,65–68], led us to hypothesize that mimicking the
576 natural environment of the toxins during their cytotoxic mode of action, might facilitate exposure of
577 critical residues necessary for effective oxidative detoxification. Indeed, by lowering the pH to 4.5,
578 we could successfully detoxify both TcdA and TcdB using MCO with Cu^{2+} (Supplementary Fig. S6
579 and S7). Subsequent control experiments where each component of the MCO reaction, such as
580 H_2O_2, Cu^{2+} and pH 4.5 were tested separately, confirmed that detoxification only occurred when a
581 combination of the three components was used. Low pH alone only had a small effect on the

582 cytotoxicity of TcdA and TcdB with reductions of around 50-fold and 350-fold respectively
583 (Supplementary Fig. S2 and S3). This is in alignment with our DSF analysis (Fig. 3A and 3B)
584 showing a partial unfolding of the toxins at pH 4.5. However, 50-fold and 350-fold reductions in
585 cytotoxicity are insufficient for using the toxoids as safe vaccine antigens, as they are still extremely
586 cytotoxic. The efficacy of our novel approach was only seen when Cu^{2+} was used in the MCO
587 system, as the usual Fenton catalysts, Fe^{2+} or Fe^{3+} in the same system could only reduce the
588 cytotoxicity by 50-fold and 7-fold respectively (Table 2, Supplementary Fig. S5). These differences
589 are mainly attributed to Cu^{2+} being a more efficient ROS-generating metal ion compared to Fe^{3+} and
590 less to the ability of Cu^{2+} to bind non-specifically to proteins [69–71]. TcdA and TcdB are known to
591 bind metal ions, both having a specific Zn^{2+} binding site in the autoprotease domain (APD), a
592 requirement for autoprocessing [65]. Mn^{2+} has also been demonstrated to bind TcdA in the catalytic
593 core of the glucosyltransferase domain (GTD), which consist of a classical Rossman fold [72,73].
594 Similarly, TcdB and the closely related *C. sordellii* Lethal Toxin (TcsL) have both been shown to
595 have specific binding requirements for Mn^{2+}, Co^{2+} and Mg^{2+}, necessary for UDP-glucose hydrolysis
596 and activating their cytotoxic effects [74]. However, in the same study, Cu^{2+} was shown to be the
597 least effective metal ion for cytotoxic activation of both TcdB and TcsL among a range of tested
598 divalent metal ions. In summary, there are no reports of TcdA and TcdB having specific Cu^{2+}-
599 binding sites, and the likely reason for the Cu^{2+}-specific effects in our MCO system is due to the
600 much higher capacity of Cu^{2+}/H_2O_2 systems to generate ROS and promote oxidative damage to the
601 toxins.

602 Finally, we also determined that the molar ratios of 1:60:1000 for TcdA/B:Cu^{2+}:H_2O_2
603 respectively, were optimal for the MCO components to achieve efficient detoxification of TcdA and
604 TcdB. The concentration of H_2O_2 in our MCO system is at least 100-fold lower than previously
605 reported for detoxification of Pertussis toxin [75] and whole-cell bacteria [76], and around 1000-fold

606 lower than a hydrogen peroxide-detoxified viral vaccine [77]. Thus, the method described here for
607 detoxification of TcdA and TcdB is orders of magnitude more efficient compared to previously used
608 oxidation methods.

609

610 **4.4 Oxidatively induced structural modifications in TcdA and TcdB**

611 To assess the structural changes induced by MCO in TcdA and TcdB we conducted far-UV CD
612 to study the secondary structure and near-UV CD to study the tertiary structure. These structural
613 studies were complemented with ELISA studies of the epitope integrity with multiple monoclonal
614 antibodies, to evaluate how these structural changes would affect the antibody recognition of various
615 TcdA and TcdB epitopes. According to the far-UV CD spectra, MCO-detoxified TcdA (Fig. 4A) and
616 MCO-detoxified TcdB (Fig. 5A) both have lost the characteristic minimum at 208 nm. This indicates
617 that the MCO detoxification modifies the α-helices of TcdA and TcdB. We also see a slight loss in
618 the magnitude of the molar ellipticity over the whole CD spectrum of TcdA, likely caused by
619 increased disordered structure or some degree of precipitation [57,60]. TcdB does not show the same
620 trend, instead, we see a more intense negative peak formed around 216 nm, which we also see in the
621 thermal denaturation experiment (Fig. 2B). It should be kept in mind that the MCO-detoxified TcdA
622 and TcdB are still at pH 4.5, and therefore the CD spectral changes might also be influenced by
623 structural modifications due to pH alone. Interestingly, raising the pH of MCO-detoxified TcdB back
624 to 7.5, the CD spectrum reverts and regains a native-like far-UV CD spectrum (Fig. 5A, red line).
625 This suggests that the acidic pH and not MCO is the major contributor to the conformational change
626 of the secondary structure of TcdB seen in the far-UV CD (Fig. 5A, blue line). Unfortunately, raising
627 the pH of TcdA to neutral after MCO detoxification was not suitable for CD analysis, as it led to the
628 loss of overall CD spectrum, likely caused by precipitation.

To further study whether it is low pH, oxidative damage or the combination of both that is the main contributing factor to the changes in secondary structure seen for TcdA, we followed the progression of the far-UV CD spectrum over time intervals of 3 min. (Supplementary Fig. S9). Two sets of experiments were run, the first with TcdA at pH 4.5 only, and the second with TcdA at pH 4.5 and MCO components. We found that already in the first spectrum at 0.1 min there is a slight difference between the MCO spectrum compared to the pH 4.5 only spectrum, with the MCO spectrum showing slightly reduced signal intensity. With further incubation, the MCO spectra show a gradual loss of the characteristic minima at 208 and 218 nm, and overall lower magnitude of molar ellipticity as we also see in Fig. 4A. This progression is plateauing around 15 min after which no further changes were detected even after 2 h. The changes of the TcdA pH 4.5 CD spectrum over time (data not shown) progresses both more slowly and is less extensive compared to the MCO spectrum, suggesting that the oxidative damage caused by MCO contributes to the change in secondary structure. Lastly, we followed the near-UV CD spectrum of MCO-detoxified TcdA over time with measurements made every 3 min during the MCO reaction. It is clear that some structural changes occur in the first 6 min, with a change of both minima at 275 and 282 nm (Supplementary Fig. S10). The decrease in the near-UV CD spectral intensity in the 275 and 282 nm region for MCO-detoxified TcdA and TcdB, suggest that tyrosine/tryptophan residues are affected by the MCO (Fig. 4B and 5B). The features in this region, however, remain intact, which indicates that the modifications of the aromatic residue environment are not severe. However, the quality of the near-UV CD spectra makes it difficult to draw any definite conclusions. Nevertheless, from the CD data we can conclude that the majority of structural events caused by MCO are happening within the first 15 min of the reaction, as further incubation only showed insignificant changes in the CD spectra. Interestingly, neither TcdA nor TcdB showed sufficient reduction of cytotoxicity after 15 min of MCO. Even after 30 min of MCO we only saw around a 400-fold reduction in cytotoxicity of TcdA (Supplementary

Fig. S1). To test whether the oxidative damage from 30 min of MCO treatment would continue to cause structural modifications over time even after the MCO reaction was quenched, we stored the sample for 48 h at 5 °C and re-tested for cytotoxicity. The level of cytotoxicity was identical to the level seen immediately after the 30 min MCO, indicating that no further structural modifications happen after the MCO reaction is quenched. A likely explanation could be that after the initial oxidation during the first 15 min, seen on both far-UV and near-UV CD (Supplementary Fig. S9 and S10), there are probably minor secondary events occurring which we cannot visually follow by CD. These secondary events are not causing significant structural changes and therefore are not visible in the CD analysis.

Epitope recognition studies of TcdA and TcdB with monoclonal antibodies show that the MCO treatment is not causing detrimental modifications of the epitopes. The mAb binding to MCO-detoxified TcdA and TcdB were on average reduced around 2-fold, relative to native TcdA and TcdB. However, when comparing to formaldehyde detoxification, we see a reduction of mAb binding of around 5-fold and 3-fold for TcdA and TcdB, respectively. These results support that our novel MCO system is more epitope conserving to TcdA and TcdB compared to conventional formaldehyde treatment. That oxidation-based detoxification is more epitope conserving than formaldehyde is in line with what was previously shown for Pertussis toxin [38].

4.5 Toxoids are stable and irreversibly detoxified

The stability and irreversibility of MCO-detoxified TcdA and TcdB were studied by far-UV CD analysis and cytotoxicity testing after 4 weeks of storage at either -20 °C, 4 °C or 25 °C. At all storage conditions, there is a decrease in CD spectral intensity for both native and MCO-detoxified TcdA and TcdB after storage (Fig. 3A-F). This is likely due to protein precipitation during storage,

as the same is seen for the native toxin samples and therefore cannot be attributed to MCO. The shape of the CD spectra for MCO-detoxified TcdA and TcdB is not changed during the storage at any temperature when compared to its corresponding CD spectra at day 0, suggesting that no further structural modifications are happening during long-term storage. Interestingly, it seems that during storage at room temperature (25 °C), the MCO-detoxified samples of both TcdA and TcdB are more resistant to precipitation compared to the native toxins (Fig. 3C and 3F). By contrast, we see the same degree of precipitation for the toxins before and after MCO at -20 °C and 4 °C. Importantly, we see no reversion of cytotoxicity after 4 weeks of storage at any temperature, whereas reversion of cytotoxicity is a well-known issue for formaldehyde-detoxified toxins [33,34].

4.6 Efficacy of oxidatively modified TcdA and TcdB vaccine in mice

Our bivalent vaccine consisting of MCO-detoxified TcdA and TcdB was compared to a similar vaccine consisting of formaldehyde-detoxified toxins, by assessing their ability to protect immunized mice against a lethal *C. difficile* oral challenge and eliciting toxin-specific antibodies. Both vaccines were able to fully protect all mice against the infection (Fig. 7A) as well as concomitant disease symptoms such as diarrhea and weight loss (Fig. 7B). All unvaccinated mice developed disease symptoms and almost 40% were moribund by day 3 and were euthanized. Hence, the efficacy of the MCO vaccine was sufficient and comparable to the formaldehyde vaccine in protecting all mice from disease symptoms. Induction of serum IgG against native TcdA and TcdB was measured by ELISA (Fig. 7C and 7D) with no statistically significant differences between the mean IgG responses elicited by the MCO-detoxified or formaldehyde-detoxified vaccine, suggesting that the two methods are comparable with regards to immunogenicity. However, mice immunized with the MCO-detoxified vaccine had lower serum levels of toxin-neutralizing antibodies compared to the group receiving the

699 formaldehyde-detoxified vaccine. The mean anti-TcdA neutralizing antibody titer in the MCO
700 vaccine group was only around half of the formaldehyde vaccine group (Fig. 7E) and we failed to
701 detect anti-TcdB neutralizing antibodies in the MCO vaccine group, while low levels of neutralizing
702 activity against TcdB was detected in the sera from the formaldehyde vaccine group (Fig. 7F). The
703 results suggest that the MCO-detoxified vaccine is slightly less efficient in eliciting neutralizing
704 antibodies against TcdA and TcdB compared to the formaldehyde-detoxified vaccine.

705 Neutralizing antibodies are crucial in CDI prevention, as they recognize and bind key epitopes
706 on the toxins that prevent them from entering the host cells and causing disease symptoms [78–81].
707 Our epitope recognition studies showed significantly higher binding of various mAbs to the MCO-
708 detoxified toxins compared to formaldehyde-detoxified ones, indicating that the epitopes were closer
709 to the native state (Table 3 and 4). This is supported by previous studies showing that oxidation-based
710 detoxification of toxins, bacteria and viruses are significantly more epitope-conserving than
711 formaldehyde [38,76,77]. We, therefore, believe that this issue is caused by some other factor(s) than
712 direct modifications of key epitopes by MCO, and further optimization of our MCO-detoxification
713 method is likely needed. Neutralizing antibodies against TcdB have been shown in several hamster
714 studies to develop much more slowly than for TcdA, and require up to four immunizations over three
715 months to reach the same levels [20,21,82]. The difficulty of stimulating anti-TcdB neutralizing
716 antibodies, in general, might have contributed to the lower levels of neutralizing TcdB antibodies we
717 detected, which were also very low in the formaldehyde vaccine group.

718 In conclusion, using mild Cu^{2+}/H_2O_2-catalyzed oxidation in combination with pH-dependent
719 structural modulation we demonstrate efficient detoxification of TcdA and TcdB. The detoxification
720 resulted in a significant reduction in toxicity yet maintaining the toxoids of TcdA and TcdB
721 structurally preserved. Furthermore, our method resulted in the development of immunogenic toxoids
722 highly recognizable by an array of monoclonal antibodies against TcdA and TcdB and capable of

protecting mice against CDI. Thus, the method may very well be suitable for the creation of safe toxoid-based antigens and a potential replacement for formaldehyde detoxification in future vaccine development.

Author Contributions

AA designed, executed, supervised and participated in all experiments, collected and analyzed all data, performed toxin purification, CD, DSF, MCO and epitope recognition experiments (Figs. 1 - 7 and Tables 1 - 4), made all the figures and tables and wrote the manuscript. **MKT** designed, executed and supervised the MCO experiments (Table 2) and CD studies (Fig. 4 and 5), participated in making Fig. 1, revised and contributed intellectually to the manuscript. **SSMM** designed, performed and collected data for the stability experiments (Fig. 6). **SJN** designed the animal study and performed serum ELISA and TNA studies and collected data for Fig. 7. **ABH** contributed to the development of the methods used in the production and purification of TcdA and TcdB. **IMM** contributed with helpful intellectual suggestions at a number of meetings and by reading and editing the manuscript. **KAK** contributed by helping with ELISA studies and *in vivo* experiments and has revised and contributed to the manuscript with intellectual content and final revision. **MJB** conceived the idea of using copper ions for the metal-catalyzed oxidation and designed, supervised and funded the MCO and CD experiments, revised and contributed to the manuscript with intellectual content. **RJ** conceived the idea for oxidation-based detoxification of TcdA and TcdB, funded and administered the study, designed and supervised all experiments, revised and contributed intellectually to the manuscript. All authors have read and approved the final version to be published.

Acknowledgments

We would like to thank Susanne Jespersen at Statens Serum Institut for invaluable help with the endless culturing of Vero cells during the entire study. We gratefully acknowledge financial support from the Novo Nordisk Foundation (Grant no.: NNF17OC0029548 to RJ), the Danish Council for

748 Independent Research Technology and Production Sciences (Grant no.: DFF| FTP 4005-00082) and
749 the Lundbeck Foundation postdoctoral fellowship (Grant no.: R231-2016-3276 to MKT).
750

751 **Declarations of interest**

752 We declare no conflict of interest

References

[1] F. Lessa, Y. Mu, W. Bamberg, Z. Beldavs, G. Dumyati, J. Dunn, M. Farley, S. Holzbauer, J. Meek, E. Phipps, L. Wilson, L. Winston, J. Cohen, B. Limbago, S. Fridkin, D. Gerding, L. McDonald, Burden of *Clostridium difficile* Infection in the United States, N. Engl. J. Med. 372 (2015) 825–834.

[2] E. Balsells, T. Shi, C. Leese, I. Lyell, J. Burrows, C. Wiuff, H. Campbell, M.H. Kyaw, H. Nair, Global burden of Clostridium difficile infections: A systematic review and meta-analysis, J. Glob. Health. 9 (2019).

[3] S. Khanna, D.S. Pardi, S.L. Aronson, P. Patricia, R. Orenstein, J.L.S. Sauver, W.S. Harmsen, A.R. Zinsmeister, The Epidemiology of Community-acquired Clostridium difficile infection: A population-based study, Am. J. Gastroenterol. 107 (2012) 89–95.

[4] M. Rupnik, M.H. Wilcox, D.N. Gerding, *Clostridium difficile* infection: new developments in epidemiology and pathogenesis, Nat. Publ. Gr. 7 (2009) 526–536.

[5] D. Wu, A. Joyee, S. Nandagopal, M. Lopez, X. Ma, J. Berry, F. Lin, Effects of *Clostridium difficile* Toxin A and B on Human T Lymphocyte Migration, Toxins (Basel). 5 (2013) 926–938.

[6] R.N. Pruitt, B. Chagot, M. Cover, W.J. Chazin, B. Spiller, D.B. Lacy, Structure-Function Analysis of Inositol Hexakisphosphate-induced Autoprocessing in Clostridium difficile Toxin A, J. Biol. Chem. 284 (2009) 21934–21940.

[7] D.E. Voth, J.D. Ballard, Clostridium difficile Toxins: Mechanism of Action and Role in Disease, Clin. Microbiol. Rev. 18 (2005) 247–263.

[8] D.M. Lyerly, K.E. Saum, D.K. Macdonald, T.D. Wilkins, Effects of Clostridium difficile Toxins Given Intragastrically to Animals, Infect. Immun. 47 (1985) 349–352.

[9] C. Fiorentini, A. Fabbri, L. Falzano, A. Fattorossi, P. Matarrese, R. Rivabene, G. Donelli,

Clostridium difficile Toxin B Induces Apoptosis in Intestinal Cultured Cells, Infect. Immun. 66 (1998) 2660–2665.

[10] M. Riegler, R. Sedivy, C. Pothoulakis, G. Hamilton, J. Zacherl, G. Bischof, E. Cosentini, W. Feil, R. Schiessel, J.T. Lamont, E. Wenzl, *Clostridium difficile* Toxin B Is More Potent than Toxin A in Damaging Human Colonic Epithelium In Vitro, J. Clin. Invest. 95 (2011) 2004–2011.

[11] G.P. Carter, J.I. Rood, D. Lyras, The role of toxin A and toxin B in *Clostridium difficile*-associated disease: Past and present perspectives., Gut Microbes. 1 (2010) 58–64.

[12] S.A. Kuehne, S.T. Cartman, J.T. Heap, M.L. Kelly, A. Cockayne, N.P. Minton, The role of toxin A and toxin B in *Clostridium difficile* infection, Nature. 467 (2010) 711–713.

[13] Z. Peng, L. Ling, C.W. Stratton, C. Li, C.R. Polage, B. Wu, Y.W. Tang, Advances in the diagnosis and treatment of Clostridium difficile infections review-article, Emerg. Microbes Infect. 7 (2018).

[14] Z. Peng, D. Jin, H.B. Kim, C.W. Stratton, B. Wu, Y.-W. Tang, X. Sun, Update on Antimicrobial Resistance in Clostridium difficile: Resistance Mechanisms and Antimicrobial Susceptibility Testing, J. Clin. Microbiol. 55 (2017) 1998–2008.

[15] P. Spigaglia, Recent advances in the understanding of antibiotic resistance in *Clostridium difficile* infection, Ther. Adv. Infect. Dis. 3 (2016) 23–42.

[16] S. Johnson, Recurrent *Clostridium difficile* infection: A review of risk factors, treatments, and outcomes, J. Infect. 58 (2009) 403–410.

[17] J. Freeman, S.D. Baines, K. Saxton, M.H. Wilcox, Effect of metronidazole on growth and toxin production by epidemic *Clostridium difficile* PCR ribotypes 001 and 027 in a human gut model, J. Antimicrob. Chemother. 60 (2007) 83–91.

[18] E. van Nood, P. Speelman, E.J. Kuijper, J.J. Keller, Struggling with recurrent Clostridium

802 difficile infections: is donor faeces the solution?, Eurosurveillance. 14 (2009).
803 [19] E. Gough, H. Shaikh, A.R. Manges, Systematic Review of Intestinal Microbiota
804 Transplantation (Fecal Bacteriotherapy) for Recurrent *Clostridium difficile* Infection, Clin.
805 Infect. Dis. 53 (2011) 994–1002.
806 [20] R.G.K. Donald, M. Flint, N. Kalyan, E. Johnson, S.E. Witko, C. Kotash, P. Zhao, S. Megati,
807 I. Yurgelonis, P.K. Lee, Y. V Matsuka, E. Severina, A. Deatly, M. Sidhu, K.U. Jansen, N.P.
808 Minton, A.S. Anderson, A novel approach to generate a recombinant toxoid vaccine against
809 *Clostridium difficile*., Microbiology. 159 (2013) 1254–66.
810 [21] N.G. Anosova, A.M. Brown, L. Li, N. Liu, L.E. Cole, J. Zhang, H. Mehta, H. Kleanthous,
811 Systemic antibody responses induced by a two-component *Clostridium difficile* toxoid
812 vaccine protect against C. difficile-associated disease in hamsters, J. Med. Microbiol. 62
813 (2013) 1394–1404.
814 [22] G. Foglia, S. Shah, C. Luxemburger, P.J. Freda, *Clostridium difficile*: Development of a
815 novel candidate vaccine, Vaccine. 30 (2012) 4307–4309.
816 [23] S. Sougioultzis, L. Kyne, D. Drudy, S. Keates, S. Maroo, C. Pothoulakis, P.J. Giannasca,
817 C.K. Lee, M. Warny, T.P. Monath, C.P. Kelly, *Clostridium difficile* toxoid vaccine in
818 recurrent C. difficile-associated diarrhea, Gastroenterology. 128 (2005) 764–770.
819 [24] H. Qiu, R. Cassan, D. Johnstone, X. Han, A.G. Joyee, M. McQuoid, A. Masi, J. Merluza, B.
820 Hrehorak, R. Reid, K. Kennedy, B. Tighe, C. Rak, M. Leonhardt, B. Dupas, L. Saward, J.D.
821 Berry, C.L. Nykiforuk, Novel *clostridium difficile* anti- Toxin (TcdA and TcdB) humanized
822 monoclonal antibodies demonstrate in vitro neutralization across a broad spectrum of clinical
823 strains and in vivo potency in a hamster spore challenge model, PLoS One. 11 (2016) 1–21.
824 [25] A.J. Marozsan, D. Ma, K.A. Nagashima, B.J. Kennedy, Y.K. Kang, R.R. Arrigale, G.P.
825 Donovan, W.W. Magargal, P.J. Maddon, W.C. Olson, Protection against *clostridium difficile*

826 infection with broadly neutralizing antitoxin monoclonal antibodies, J. Infect. Dis. 206
827 (2012) 706–713.
828 [26] ClinicalTrials.gov Identifier: NCT02316470, (n.d.).
829 [27] ClinicalTrials.gov Identifier: NCT03918629, (n.d.).
830 [28] ClinicalTrials.gov Identifier: NCT01887912, (n.d.).
831 [29] T.-A. Morten, B.J. Sys, S.W. Ellen, W.P. Jesper, H. Peter, Investigation of the detoxification
832 mechanism of formaldehyde-treated tetanus toxin, Vaccine. 25 (2007) 2213–2227.
833 [30] C. Neumüller, Detoxification of Diphtheria Toxin with Formaldehyde mixed with an Amino-
834 Acid, Nature. 174 (1954) 405–406.
835 [31] R.K. Gupta, S.B. Sharma, S. Ahuja, S.N. Saxena, The effects of different inactivating agents
836 on the potency, toxicity and stability of pertussis vaccine, J. Biol. Stand. 15 (1987) 87–98.
837 [32] FDA, Vaccines Licensed for Use in the United States, 2019. (n.d.).
838 https://www.fda.gov/vaccines-blood-biologics/vaccines/vaccines-licensed-use-united-states.
839 [33] D.S. Thiriot, G. Dornadula, A. Kristopeit, B. Wang, L. Hong, H. Mach, S. Wang, A.
840 Kanavage, J.T. Blue, F. Wang, C.D. Mensch, R.R. Rustandi, S. Secore, J.H. Heinrichs,
841 Detecting and preventing reversion to toxicity for a formaldehyde-treated *C. difficile* toxin B
842 mutant, Vaccine. 33 (2014) 252–259.
843 [34] E. Vidunas, A. Mathews, M. Weaver, P. Cai, E.H. Koh, S. Patel-Brown, H. Yuan, Z. rong
844 Zheng, M. Carriere, J.E. Johnson, J. Lotvin, J. Moran, Production and Characterization of
845 Chemically Inactivated Genetically Engineered *Clostridium difficile* Toxoids, J. Pharm. Sci.
846 105 (2016) 2032–2041.
847 [35] R.C. Grafstrom, A.J. Fornace, H. Autrup, J.F. Lechner, C.C. Harris, Formaldehyde damage
848 to DNA and inhibition of DNA repair in human bronchial cells, Science (80-.). 220 (1983)
849 216–218.

[36] M. Soffritti, C. Maltoni, F. Maffei, R. Biagi, Formaldehyde: An experimental multipotential carcinogen, Toxicol. Ind. Health. 5 (1989) 699–730.

[37] R.G.A. Jones, Y. Liu, P. Rigsby, D. Sesardic, An improved method for development of toxoid vaccines and antitoxins, J. Immunol. Methods. 337 (2008) 42–48. https://doi.org/10.1016/j.jim.2008.05.009.

[38] P.H. Ibsen, The effect of formaldehyde, hydrogen peroxide and genetic detoxification of pertussis toxin on epitope recognition by murine monoclonal antibodies, Vaccine. 14 (1996) 359–368.

[39] A. Di Tommaso, M.T. De Magistris, M. Bugnoli, I. Marsili, R. Rappuoli, S. Abrignani, Formaldehyde treatment of proteins can constrain presentation to T cells by limiting antigen processing, Infect. Immun. 62 (1994) 1830–1834.

[40] L. Chen, M. Tang, C. Chen, M. Chen, K. Luo, J. Xu, D. Zhou, F. Wu, Efficient Bacterial Inactivation by Transition Metal Catalyzed Auto-Oxidation of Sulfite, Environ. Sci. Technol. 51 (2017) 12663–12671.

[41] R.A. Clark, Oxidative inactivation of pneumolysin by the myeloperoxidase system and stimulated human neutrophils, J. Immunol. 136 (1986) 4617–4622.

[42] A. Jekle, J. Yoon, M. Zuck, R. Najafi, L. Wang, T. Shiau, C. Francavilla, S.A. Rani, C. Eitzinger, M. Nagl, M. Anderson, D. Debabov, NVC-422 inactivates staphylococcus aureus toxins, Antimicrob. Agents Chemother. 57 (2013) 924–929.

[43] G.R. Siber, N. Thakrar, B.A. Yancey, L. Herzog, C. Todd, N. Cohen, R.D. Sekura, C.U. Lowe, Safety and immunogenicity of hydrogen peroxide-inactivated pertussis toxoid in 18-month-old children, Vaccine. 9 (1991) 735–740.

[44] I. Krantz, R. Sekura, B. Trollfors, J. Taranger, G. Zackrisson, T. Lagergard, R. Schneerson, J. Robbins, Immunogenicity and safety of a pertussis vaccine composed of pertussis toxin

874 inactivated by hydrogen peroxide, in 18- to 23-month-old children, J. Pediatr. 116 (1990)
875 539–543.
876 [45] M.K. Tiwari, F. Leinisch, C. Sahin, I.M. Møller, D.E. Otzen, M.J. Davies, M.J. Bjerrum,
877 Early events in copper-ion catalyzed oxidation of α-synuclein, Free Radic. Biol. Med. 121
878 (2018) 38–50.
879 [46] M.K. Tiwari, P.M. Hägglund, I.M. Møller, M.J. Davies, M.J. Bjerrum, Copper ion / H2O2
880 oxidation of Cu/Zn-Superoxide dismutase: Implications for enzymatic activity and
881 antioxidant action, Redox Biol. 26 (2019) 101262.
882 [47] L. Wentzel, M. Sterne, A. Polson, High toxicity of pure botulinum type D toxin, Nature. 166
883 (1950) 739–740.
884 [48] S. Boivin, S. Kozak, R. Meijers, Optimization of protein purification and characterization
885 using Thermofluor screens, Protein Expr. Purif. 91 (2013) 192–206.
886 [49] Ammerman, Vero cell line maintenance, Curr Protoc Microbiol. (2009) 1–10.
887 [50] X. Chen, K. Katchar, J.D. Goldsmith, N. Nanthakumar, A. Cheknis, D.N. Gerding, C.P.
888 Kelly, A Mouse Model of *Clostridium difficile*-Associated Disease, Gastroenterology. 135
889 (2008) 1984–1992.
890 [51] L.T. Erikstrup, M. Aarup, R. Hagemann-Madsen, F. Dagnaes-Hansen, B. Kristensen, K.E.P.
891 Olsen, K. Fuursted, Treatment of *Clostridium difficile* infection in mice with vancomycin
892 alone is as effective as treatment with vancomycin and metronidazole in combination, BMJ
893 Open Gastroenterol. 2 (2015) 1–9.
894 [52] H. Krivan, T. Wilkins, Purification of *Clostridium difficile* Toxin A by Affinity, Infect.
895 Immun. 55 (1987) 1873–1877.
896 [53] S.W. Fu, J. Xue, Y.L. Zhang, D.Y. Zhou, Simplified purification method for *Clostridium*
897 *difficile* toxin A, World J. Gastroenterol. 10 (2004) 2756–2758.

[54] T. Ookawara, N. Kawamura, Y. Kitagawa, N. Taniguchi, Site-specific and random fragmentation of Cu,Zn-superoxide dismutase by glycation reaction. Implication of reactive oxygen species, J. Biol. Chem. 267 (1992) 18505–18510.

[55] S. Goldstein, D. Meyerstein, Commentary: Comments on the mechanism of the "Fenton-like" reaction, Acc. Chem. Res. 32 (1999) 547–550.

[56] D. Corrêa, C. Ramos, The use of circular dichroism spectroscopy to study protein folding, form and function, African J Biochem Res. 3 (2009) 164–173.

[57] M.S. Salnikova, S.B. Joshi, J.H. Rytting, M. Warny, C.R. Middaugh, Physical characterization of clostridium difficile toxins and toxoids: Effect of the formaldehyde crosslinking on thermal stability, J. Pharm. Sci. 97 (2008) 3735–3752.

[58] N.M. Chumbler, S.A. Rutherford, Z. Zhang, M.A. Farrow, J.P. Lisher, E. Farquhar, D.P. Giedroc, B.W. Spiller, R.A. Melnyk, D.B. Lacy, Crystal structure of *Clostridium difficile* toxin A, Nat. Microbiol. 1 (2016) 1–15.

[59] P. Chen, K. Lam, Z. Liu, F.A. Mindlin, B. Chen, C.B. Gutierrez, L. Huang, Y. Zhang, T. Hamza, H. Feng, T. Matsui, M.E. Bowen, K. Perry, R. Jin, Structure of the full-length *Clostridium difficile* toxin B, Nat. Struct. Mol. Biol. 26 (2019) 712–719.

[60] K. Matsuo, Y. Sakurada, R. Yonehara, M. Kataoka, K. Gekko, Secondary-structure analysis of denatured proteins by vacuum-ultraviolet circular dichroism spectroscopy, Biophys. J. 92 (2007) 4088–4096.

[61] B. Shivu, S. Seshadri, J. Li, K.A. Oberg, V.N. Uversky, A.L. Fink, Distinct β-sheet structure in protein aggregates determined by ATR-FTIR spectroscopy, Biochemistry. 52 (2013) 5176–5183.

[62] O. Gursky, S. Aleshkov, Temperature-dependent β-sheet formation in β-amyloid Aβ1-40 peptide in water: Uncoupling β-structure folding from aggregation, Biochim. Biophys. Acta -

Protein Struct. Mol. Enzymol. 1476 (2000) 93–102.

[63] F. Ding, J.J. LaRocque, N. V. Dokholyan, Direct observation of protein folding, aggregation, and a prion-like conformational conversion, J. Biol. Chem. 280 (2005) 40235–40240.

[64] J. Tam, G.L. Beilhartz, A. Auger, P. Gupta, A.G. Therien, R.A. Melnyk, Small Molecule Inhibitors of Clostridium difficile Toxin B-Induced Cellular Damage, Chem. Biol. 22 (2015) 175–185.

[65] R.N. Pruitt, M.G. Chambers, K.K.-S. Ng, M.D. Ohi, D.B. Lacy, Structural organization of the functional domains of Clostridium difficile toxins A and B, Proc. Natl. Acad. Sci. 107 (2010) 13467–13472.

[66] M. Qa'dan, L.M. Spyres, J.D. Ballard, pH-induced conformational changes in *Clostridium difficile* toxin B, Infect. Immun. 68 (2000) 2470–2474.

[67] T. Giesemann, T. Jank, R. Gerhard, E. Maier, I. Just, R. Benz, K. Aktories, Cholesterol-dependent pore formation of *Clostridium difficile* toxin A, J. Biol. Chem. 281 (2006) 10808–10815.

[68] H. Barth, G. Pfeifer, F. Hofmann, E. Maier, R. Benz, K. Aktories, Low ph-induced Formation of Ion Channels by *Clostridium difficile* Toxin B in Target Cells, J. Biol. Chem. 276 (2001) 10670–10676.

[69] L. Pecci, G. Montefoschi, D. Cavallini, Some new details of the copper-hydrogen peroxide interaction, Biochem. Biophys. Res. Commun. 235 (1997) 264–267.

[70] M.E. Letelier, S. Sánchez-Jofré, L. Peredo-Silva, J. Cortés-Troncoso, P. Aracena-Parks, Mechanisms underlying iron and copper ions toxicity in biological systems: Pro-oxidant activity and protein-binding effects, Chem. Biol. Interact. 188 (2010) 220–227.

[71] O.I. Aruoma, B. Halliwell, E. Gajewski, M. Dizdaroglu, Copper-ion-dependent damage to the bases in DNA in the presence of hydrogen peroxide, Biochem. J. 273 (1991) 601–604.

946 https://doi.org/10.1042/bj2730601.
947 [72] R.N. Pruitt, N.M. Chumbler, S.A. Rutherford, M.A. Farrow, D.B. Friedman, B. Spiller, D.B.
948 Lacy, Structural determinants of Clostridium difficile toxin A glucosyltransferase activity, J.
949 Biol. Chem. 287 (2012) 8013–8020.
950 [73] N. D'Urzo, E. Malito, M. Biancucci, M.J. Bottomley, D. Maione, M. Scarselli, M. Martinelli,
951 The structure of *Clostridium difficile* toxin A glucosyltransferase domain bound to Mn2+
952 and UDP provides insights into glucosyltransferase activity and product release, FEBS J. 279
953 (2012) 3085–3097.
954 [74] H. Genth, I. Schelle, I. Just, Metal ion activation of *clostridium sordellii* lethal Toxin and
955 *clostridium difficile* Toxin B, Toxins (Basel). 8 (2016).
956 [75] R.D. Sekura, Novel method of preparing toxoid by oxidation and metal ions, US4762710A,
957 1988. https://patents.google.com/patent/WO1987007507A1/en.
958 [76] Y. Fan, Y. Mu, L. Lu, Y. Tian, F. Yuan, B. Zhou, C. Yu, Z. Wang, X. Li, S. Lei, Y. Xu, D.
959 Wu, L. Yang, Hydrogen peroxide-inactivated bacteria induces potent humoral and cellular
960 immune responses and releases nucleic acids, Int. Immunopharmacol. 69 (2019) 389–397.
961 [77] I.J. Amanna, H.-P. Raué, M.K. Slifka, Development of a new hydrogen peroxide–based
962 vaccine platform, Nat. Med. 18 (2012) 974–979.
963 [78] G.J. Babcock, T.J. Broering, H.J. Hernandez, R.B. Mandell, K. Donahue, N. Boatright, A.M.
964 Stack, I. Lowy, R. Graziano, D. Molrine, D.M. Ambrosino, W.D. Thomas, I.N.I. Mmun,
965 Human Monoclonal Antibodies Directed against Toxins A and B Prevent Clostridium
966 difficile-Induced Mortality in Hamsters, Infect. Immun. 74 (2006) 6339–6347.
967 [79] G. Corthier, M.C. Muller, T.D. Wilkins, D. Lyerly, R. L'Hardion, Protection against
968 experimental pseudomembranous colitis in gnotobiotic mice by use of monoclonal antibodies
969 against *Clostridium difficile* toxin A, Infect. Immun. 59 (1991) 1192–1195.

970 [80] J.F. Torres, D.M. Lyerly, J.E. Hill, T.P. Monath, Evaluation of formalin-inactivated
971 *Clostridium difficile* vaccines administered by parenteral and mucosal routes of
972 immunization in hamsters, Infect. Immun. 63 (1995) 4619–4627.
973 [81] I. Lowy, D.C. Molrine, B.A. Leav, B.M. Blair, R. Baxter, D.N. Gerding, G. Nichol, W.D.
974 Thomas, M. Leney, S. Sloan, C.A. Hay, D.M. Ambrosino, Treatment with monoclonal
975 antibodies against *Clostridium difficile* toxins., N. Engl. J. Med. 362 (2010) 197–205.
976 [82] S. Secore, S. Wang, J. Doughtry, J. Xie, M. Miezeiewski, R.R. Rustandi, M. Horton, R.
977 Xoconostle, B. Wang, C. Lancaster, A. Kristopeit, S.C. Wang, S. Christanti, S. Vitelli, M.P.
978 Gentile, A. Goerke, J. Skinner, E. Strable, D.S. Thiriot, J.L. Bodmer, J.H. Heinrichs,
979 Development of a novel vaccine containing binary toxin for the prevention of *Clostridium*
980 *difficile* disease with enhanced efficacy against NAP1 strains, PLoS One. 12 (2017) 1–23.
981
982

Supplementary Information

Detoxification of Toxin A and Toxin B by copper ion-catalyzed oxidation in production of a toxoid-based vaccine against *Clostridioides difficile*

Aria Aminzadeh[1,2,§], Manish K. Tiwari[2,§], Srwa Satar Mamah Mustapha[1], Sandra Junquera Navarrete[1], Anna Bielecka Henriksen[1], Ian Max Møller[3], Karen Angeliki Krogfelt[4], Morten Jannik Bjerrum[2], René Jørgensen[1,*]

[1]Statens Serum Institut, Department of Bacteria, Parasites and Fungi, Copenhagen, Denmark

[2]University of Copenhagen, Department of Chemistry, Copenhagen, Denmark

[3]Department of Molecular Biology and Genetics, Aarhus University, Forsøgsvej 1, DK-4200 Slagelse, Denmark

[4]Roskilde University, Molecular and Medical Biology, Roskilde Denmark

*Correspondence to: renj@ssi.dk

René Jørgensen

Statens Serum Institut, Department of Bacteria, Parasites and Fungi,

Artillerivej 5, 2300 Copenhagen S, Denmark

Contents

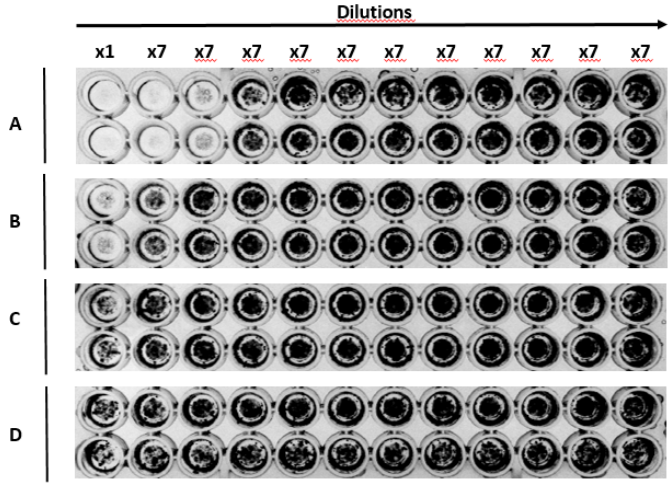

1021

1022 **Fig. S1. *In vitro* cytotoxicity on Vero cells of TcdA detoxified by MCO using different incubation times.** Microtiter
1023 plates were stained with crystal violet after 48 h incubation and photographed to visualize cell survival (black wells). All
1024 samples were tested as duplicates and consisted of 2 µg MCO-detoxified TcdA added to the first column and serially
1025 diluted horizontally. All samples were incubated at 37°C. **A)** 30 min **B)** 60 min **C)** 90 min **D)** 120 min.

1026

1027

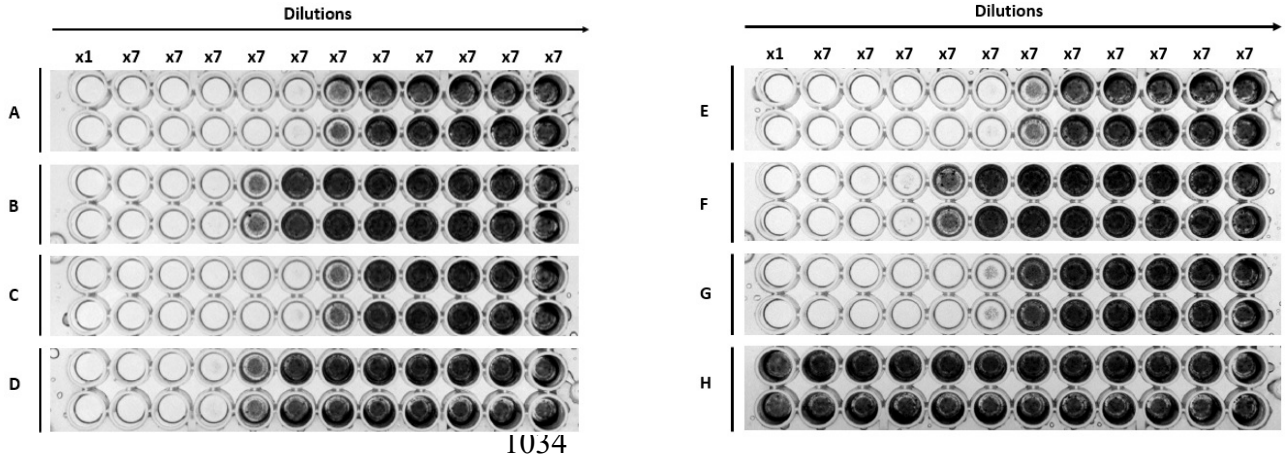

1034

1035 **Fig. S2. *In vitro* cytotoxicity on Vero cells of MCO control samples with TcdA.** Plates were stained as described in
1036 Fig S1. All samples were tested as duplicates and consisted of 1.9 µg TcdA added to first column and serially diluted
1037 horizontally. All samples were incubated for 2 h at 37 °C. **A)** Native TcdA in pH 7.5 **B)** Native TcdA in pH 4.5 **C)** TcdA
1038 + H_2O_2 in pH 7.5 **D)** TcdA + H_2O_2 in pH 4.5 **E)** TcdA + $CuCl_2$ in pH 7.5 **F)** TcdA + $CuCl_2$ in pH 4.5 **G)** TcdA + H_2O_2 +
1039 $CuCl_2$ in pH 7.5 (MCO) **H)** TcdA + H_2O_2 + $CuCl_2$ in pH 4.5 (MCO).

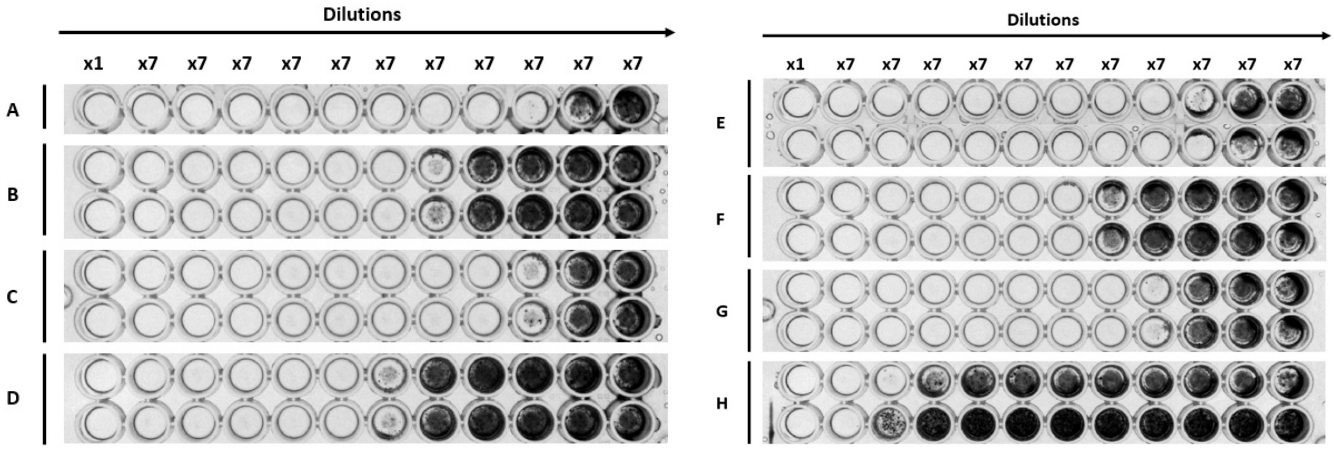

Fig. S3. ***In vitro*** **cytotoxicity on Vero cells of MCO control samples with TcdB.** Plates were stained with crystal violet after 48 h incubation and photographed to visualize cell survival in each well with black stain. All samples were tested as duplicates and consisted of 1.75 µg TcdB added to first column and serially diluted horizontally. All samples were incubated for 2 h at 37 °C. **A)** Native TcdB in pH 7.5 **B)** Native TcdB in pH 4.5 **C)** TcdB + H_2O_2 in pH 7.5 **D)** TcdB + H_2O_2 in pH 4.5 **E)** TcdB + $CuCl_2$ in pH 7.5 **F)** TcdB + $CuCl_2$ in pH 4.5 **G)** TcdB + H_2O_2 + $CuCl_2$ in pH 7.5 (MCO) **H)** TcdB + H_2O_2 + $CuCl_2$ in pH 4.5 (MCO).

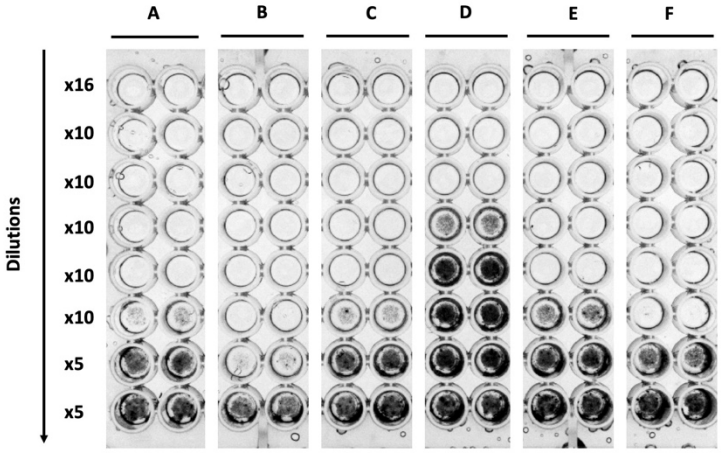

Fig. S4. ***C. difficile*** **toxin yield in various growth media tested on Vero cells.** Samples were taken from each culture after 48 hours of growth, centrifuged and filtered. Ten µL was added to the first row (x16) and serially diluted vertically. Plates were stained with crystal violet after 48 h incubation and photographed to visualize cell survival in each well with black stain. All samples were tested as duplicates and consisted of 20 g/L yeast extract, 1 g/L sodium thioglycolate and 30 g/L of either **A)** NZ-Soy **B)** NZ-Soy BL4 **C)** NZ-Soy BL7 **D)** Phytone peptone **E)** BHI **G)** Tryptone.

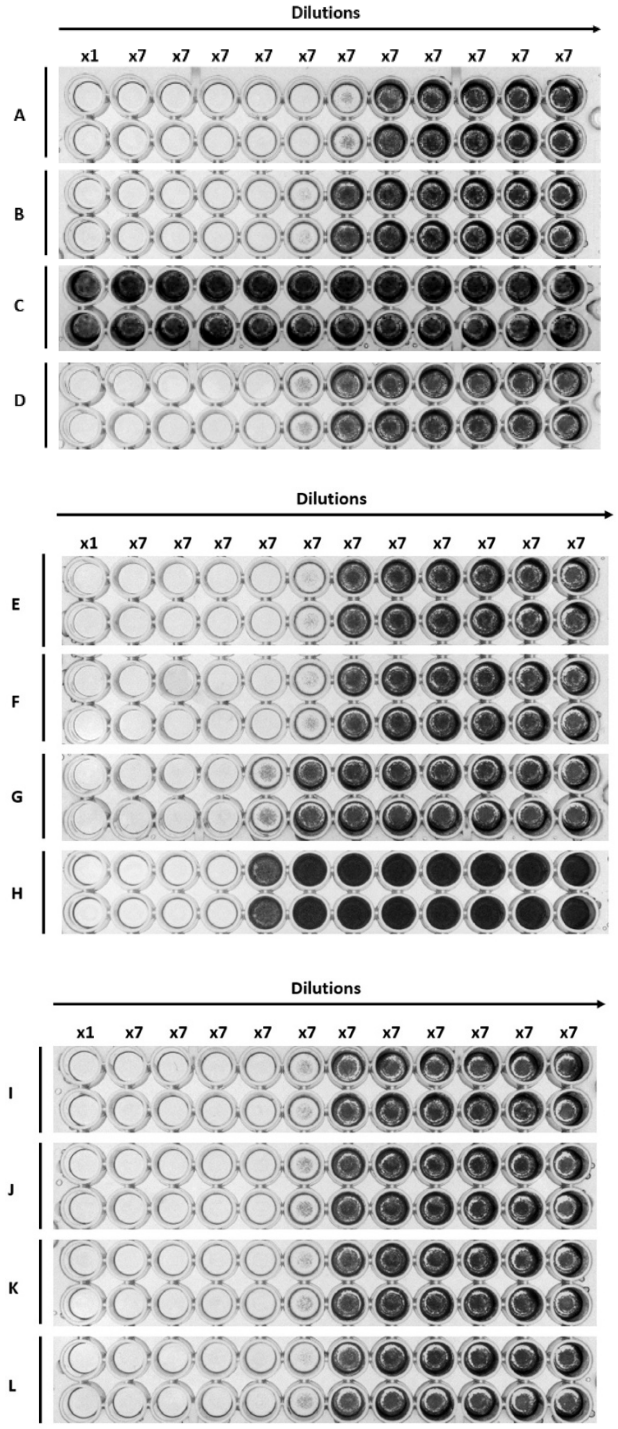

Fig. S5. ***In vitro*** **cytotoxicity on Vero cells of TcdA detoxified by MCO using different metal ions.** Plates were stained with crystal violet after 48 h incubation and photographed to visualize cell survival in each well with black stain. All samples were tested as duplicates and consisted of 3.2 µg MCO-detoxified TcdA added to first column, and serially diluted horizontally. All samples were incubated for 2 h at 37 °C prior to cytotoxicity testing. All MCO samples were in pH 4.5. **A)** TcdA in pH 7.5 **B)** TcdA in pH 4.5 **C)** TcdA MCO + $CuCl_2$ **D)** TcdA MCO + $MgCl_2$ **E)** TcdA MCO + $CoCl_2$ **F)** TcdA MCO + $MnCl_2$ **G)** TcdA MCO + $Fe_2(SO_4)_3$ **H)** TcdA MCO + $FeSO_4$ **I)** TcdA MCO + $CaCl_2$ **J)** TcdA MCO + LiCl **K)** TcdA MCO + $NiCl_2$ **L)** TcdA MCO + $AgNO_3$.

1057

1058

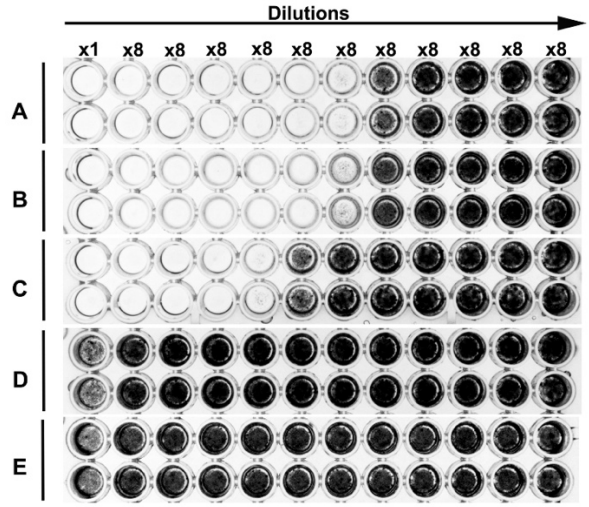

Fig. S6. *In vitro* cytotoxicity on Vero cells of native and MCO-detoxified TcdA. Plates were stained with crystal violet after 48 h incubation and photographed to visualize cell survival in each well with black stain. All samples were tested as duplicates and consisted of 3.7 µg native or MCO-detoxified TcdA added to the first column and serially diluted horizontally. All samples were incubated for 2 h at 37 °C. **A)** Native TcdA in pH 7.5 **B)** MCO-detoxified TcdA in pH 7.5 **C)** Native TcdA in pH 4.5 **D)** MCO-detoxified TcdA in pH 4.5 **E)** MCO-detoxified TcdA in pH 4.5 re-adjusted to pH 7.5.

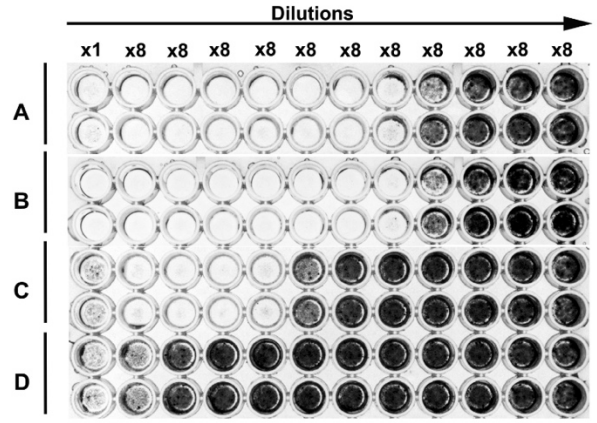

Fig. S7. *In vitro* cytotoxicity on Vero cells of native and MCO-detoxified TcdB. Plates were stained with crystal violet after 48 h incubation and photographed to visualize cell survival in each well with black stain All samples were tested as duplicates and consisted of 2.2 µg native or MCO-detoxified TcdB added to the first column and serially diluted horizontally. All samples were incubated for 2 h at 37 °C. **A)** Native TcdB in pH 7.5 **B)** MCO-detoxified TcdB in pH 7.5, **C)** Native TcdB in pH 4.5 **D)** MCO-detoxified TcdB in pH 4.5 re-adjusted to pH 7.5.

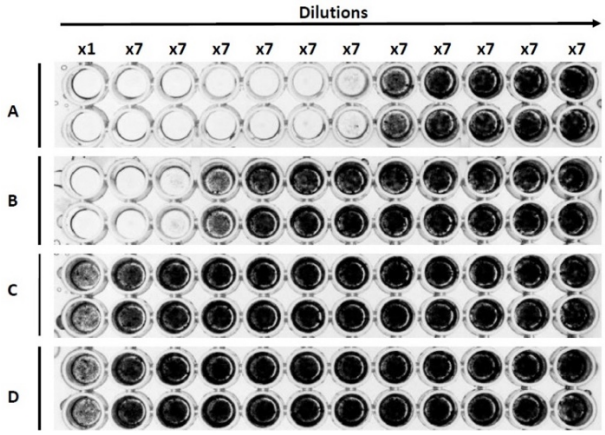

Fig. S8. *In vitro* cytotoxicity on Vero cells of TcdA detoxified by MCO at varying temperatures. Plates were stained with crystal violet after 48 h incubation and photographed to visualize cell survival in each well with black stain. All samples were tested as duplicates and consisted of 3.2 µg TcdA added to the first column and serially diluted horizontally. All samples were incubated for 90 min. **A)** Native TcdA in pH 7.5, **B)** MCO-detoxified TcdA 25 °C, **C)** MCO-detoxified TcdA 30 °C, **D)** MCO-detoxified TcdA 37 °C.

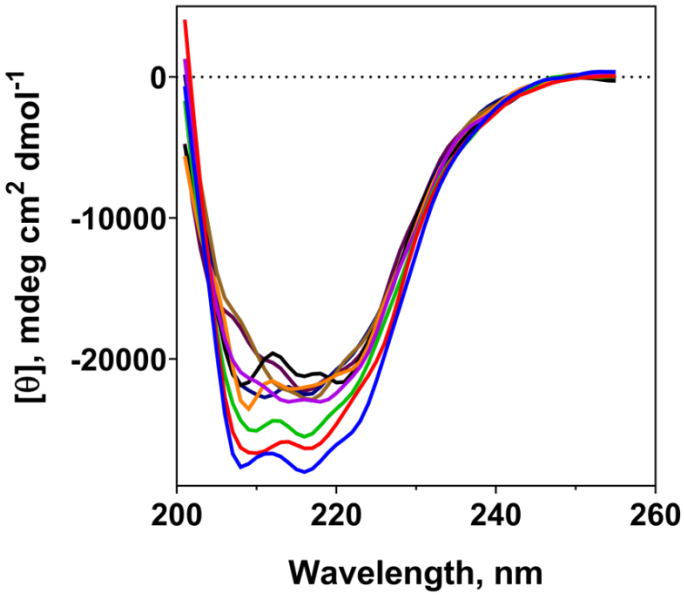

Fig. S9. Far-UV circular dichroism analysis of the structural effect of MCO detoxification on TcdA. All samples are shown as an average of duplicate measurements with the buffer spectrum (blank) subtracted. The sample consisted of 0.65 µM TcdA. Far-UV spectra ranging from 200 – 255 nm. Blue: Native TcdA pH 4.5 0.1 min, red: TcdA MCO 0.1 min, green: TcdA MCO 3 min, purple: TcdA MCO 6 min, orange: TcdA MCO 9 min, black: TcdA MCO 12 min, brown: TcdA MCO 15 min, dark blue: TcdA MCO 18 min, magenta: TcdA MCO 21 min.

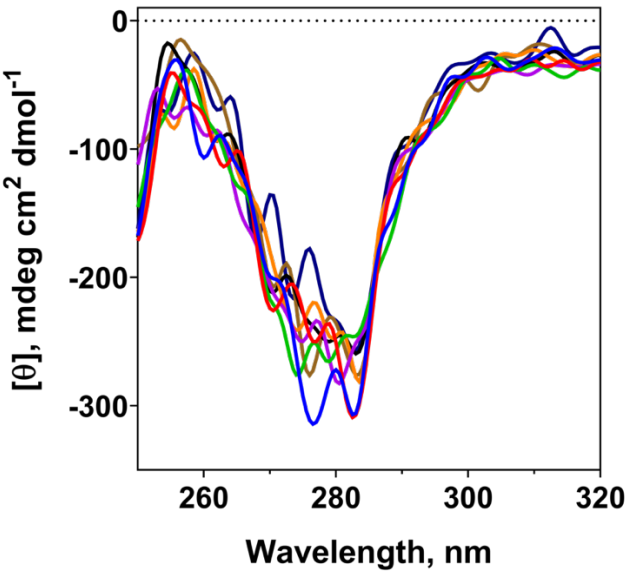

Fig. S10. Near-UV circular dichroism analysis of the structural effect of MCO detoxification on TcdA. All samples are shown as an average of duplicate measurements with the buffer spectrum (blank) subtracted. Sample consisted of 3.25 µM TcdA. Near-UV spectra ranging from 250 – 320 nm. Blue: TcdA MCO 0.1 min, red: TcdA MCO 3 min, green: TcdA MCO 6 min, purple: TcdA MCO 9 min, orange: TcdA MCO 12 min, black: TcdA MCO 15 min, brown: TcdA MCO 18 min, dark blue: TcdA MCO 21 min.

1096 **Table S1. Molar ratios and experimental conditions used for the MCO pilot study on TcdA.**

Samples	Final concentrations in reaction mixture (μM)			Molar ratios	pH
	TcdA	$CuCl_2$	H_2O_2	(TcdA:Cu^{2+}:H_2O_2)	(tested at all pH)
Condition 1	0.5	15	50	1:30:100	4, 4.5, 5, 7.5*
Condition 2	0.5	15	250	1:30:500	4, 4.5, 5, 7.5
Condition 3	0.5	15	500	1:30:1000	4, 4.5, 5, 7.5
Condition 4	0.5	30	50	1:60:100	4, 4.5, 5, 7.5
Condition 5	0.5	30	500	1:60:1000	4, 4.5, 5, 7.5
Condition 6	0.5	37.5	250	1:75:500	4, 4.5, 5, 7.5
Condition 7	0.5	37.5	500	1:75:1000	4, 4.5, 5, 7.5
Condition 8	0.5	37.5	1000	1:75:2000	4, 4.5, 5, 7.5

* = All four pH values were tested for each condition.

1097